Molecular Mechanisms that Stabilize Short Term Synaptic Plasticity During Presynaptic Homeostatic Plasticity

Jennifer M. Ortega, Ozgur Genç and Graeme W. Davis*

Department of Biochemistry and Biophysics
Kavli Institute for Fundamental Neuroscience
Rock Hall, 4th Floor North Rm 448E
University of California, San Francisco
San Francisco, CA 94158
graeme.davis@ucsf.edu

*to whom correspondence should be addressed

Number of pages: 50
Number of figures: 9
Number of Supplemental files: 1
Number of Supplemental figures: 1

ABSTRACT

Presynaptic homeostatic plasticity (PHP) compensates for impaired postsynaptic neurotransmitter receptor function through a rapid, persistent adjustment of neurotransmitter release, an effect that can exceed 200%. An unexplained property of PHP is the preservation of short-term plasticity (STP), thereby stabilizing activity-dependent synaptic information transfer. We demonstrate that the dramatic potentiation of presynaptic release during PHP is achieved while simultaneously maintaining a constant ratio of primed to super-primed synaptic vesicles, thereby preserving STP. Mechanistically, genetic, biochemical and electrophysiological evidence argue that a constant ratio of primed to super-primed synaptic vesicles is achieved by the concerted action of three proteins: Unc18, Syntaxin1A and RIM. Our data support a model based on the regulated availability of Unc18 at the presynaptic active zone, a process that is restrained by Syntaxin1A and facilitated by RIM. As such, regulated vesicle priming/super-priming enables PHP to stabilize both synaptic gain and the activity-dependent transfer of information at a synapse.

INTRODUCTION

Presynaptic homeostatic plasticity (PHP) is an evolutionarily conserved form of homeostatic control that is expressed in organisms ranging from fly to human (Cull-Candy et al., 1980; Plomp et al., 1992; Davis, 2013; Wang et al., 2011), at both central and peripheral synapses (Liu and Tsien, 1995; Davis and Goodman, 1998; Burrone et al., 2002; Thiagarajan et al., 2005; Kim and Ryan 2010; Zhao et al., 2011; Davis, 2013; Henry et al., 2012; Jakawich et al., 2010). PHP can be induced in less than ten minutes and is expressed as a dramatic increase in synaptic vesicle fusion (≥200%) at a fixed number of presynaptic release sites.

An unexplained, emergent property of PHP is the preservation of short-term release dynamics during a stimulus train, referred to here as short-term plasticity or 'STP' (Figure 1; see Weyhersmüller et al., 2011; Müller et al., 2012; Müller et al., 2015; Orr et al., 2017). STP is a fundamental property of neural coding, underlying behaviorally relevant circuit-level computations (Davis and Murphey, 1994). Indeed, STP is described as being *"…an almost necessary condition for the existence of (short-lived) activity states in the central nervous system*" (von der Malsburg and Bienenstock, 1986; as recently quoted in Taschenburger et al., 2016). Thus, the fact that STP is held constant during the expression of PHP may be essential to the life-long stabilization of neural circuit function and animal behavior. But, it remains fundamentally unknown how presynaptic release can be rapidly doubled at a fixed number of active zones while maintaining constant short-term release dynamics.

Two processes within the presynaptic terminal are known to be required for the homeostatic potentiation of vesicle release: 1) an increase in presynaptic calcium influx controlled by ENaC channel insertion in the presynaptic membrane (Younger et al., 2013; Orr et al., 2017) and 2) an increase in the readily releasable pool of synaptic vesicles that requires the presynaptic scaffolding proteins RIM and RBP (Müller et al., 2012; Davis and Müller, 2015; Müller et al., 2015). It has been proposed that the combined effects of elevated presynaptic calcium and an increased supply of release ready vesicles are sufficient to achieve PHP. But, current models have yet to address how short-term release dynamics are stabilized.

STP can be strongly influenced by the partition of the readily releasable vesicle pool into two functional subclasses: 1) docked vesicles that have a low intrinsic calcium sensitivity of release that are referred to as ‘primed’ and 2) docked vesicles that have a relatively higher intrinsic calcium sensitivity and are referred to as ‘super-primed’. During a stimulus train, super-primed vesicles will dominate release during the first few action potentials and primed vesicle will dominate subsequent release (Taschenburger et al., 2016; Lee et al., 2013; Müller et al., 2010). Thus, a synapse harboring a large proportion of super-primed vesicles will favor a high initial release rate followed by synaptic depression while a synapse harboring a small proportion of super-primed vesicles will be prone facilitation of release, followed by subsequent synaptic depression (Taschenburger et al., 2016; Lee et al., 2013). There is both pharmacological and genetic evidence in support of this model. Genetic mutations that impair vesicle super-priming convert depression-prone, high-

release probability synapses into low-release probability synapses that express short-term facilitation (Schluter et al., 2006; Deak et al., 2009; He et al., 2017). The calcium sensitivity of vesicle fusion is also highly sensitive to phorbol esters (PdBu), which lower the fusion barrier to release (Taschenburger et al., 2016; Lee et al., 2013). Application of PdBu, which is considered to drive the super-priming process, dramatically potentiates vesicle release and leads to enhanced short-term synaptic depression (Taschenburger et al., 2016; Lee et al., 2013).

Here, we provide evidence that the stabilization of STP during PHP is achieved by maintaining a constant ratio of primed to super-primed synaptic vesicles. First, we confirm that STP is precisely preserved during the expression of PHP. Second, we document a PdBu sensitive release mechanism at the Drosophila NMJ and provide evidence that the fraction of super-primed vesicles is maintained during the full extent of PHP. Third, we provide molecular insight into how a constant fraction of super-primed vesicles is maintained during the expression of PHP. We demonstrate that Unc18 has an evolutionarily conserved function during the rapid induction of PHP. We show that Unc18 function during PHP is facilitated by the activity of presynaptic RIM and, remarkably, is antagonized by presynaptic Syntaxin. Based upon these and other data, we present a new model for the homeostatic control of synaptic vesicle release that is based upon the regulated control of Unc18 levels at the presynaptic release site, acting in concert with the priming activity of RIM to stabilize STP in the presence of a homeostatic doubling presynaptic neurotransmitter release.

RESULTS

We begin by documenting how the short-term dynamics of presynaptic release (short-term plasticity or STP) are held constant during the expression of PHP. We rapidly induce PHP by application of sub-blocking concentrations of the glutamate receptor antagonist philanthotoxin (PhTx, 10-20μM). PhTx causes a ~50% decrease in miniature excitatory postsynaptic potential (mEPSP) amplitude and induces a homeostatic increase in presynaptic vesicle release that precisely counteracts the change in mEPSP amplitude, maintaining the amplitude of action potential evoked neurotransmitter release at baseline levels (Frank et al., 2006; Davis, 2013). As shown in Figure 1A, even at elevated extracellular calcium (3.0mM $[Ca^{2+}]_e$), excitatory postsynaptic currents (EPSC) are precisely maintained at control levels following application of PhTx (see Müller and Davis, 2012; see below for further quantification).

Next, we characterize the expression of STP at two concentrations of external calcium (0.75mM and 3.0mM $[Ca^{2+}]_e$), doing so in the presence and absence of PhTx to induce PHP (Figure 1A-C). Note that the effects of non-linear summation prevents accurate calculation of presynaptic release at calcium concentrations in excess of approximately 0.3mM. As such, measurement of synaptic currents in two electrode voltage clamp configuration are essential for experiments where extracellular calcium exceeds 0.3mM. As expected (Zucker and Reghr, 2002), STP is strongly dependent on the concentration of external calcium, showing facilitation at 0.75mM $[Ca^{2+}]_e$ and depression at 3.0mM $[Ca^{2+}]_e$ (Figure 1A, B). Application of PhTx causes an approximate doubling of presynaptic release during PHP that is similar in magnitude to the change in

release observed when comparing wild type neurotransmission at 0.75mM $[Ca^{2+}]_e$ and 3.0mM $[Ca^{2+}]_e$. However, the expression of PHP occurs without a change in release dynamics (Figure 1B, C). Specifically, there is no statistically significant change in paired pulse ratio comparing the presence and absence of PhTx, and this is true at both 0.75mM $[Ca^{2+}]_e$ where facilitation dominates (p=0.65; Student's t-test, two tailed) and at 3.0mM $[Ca^{2+}]_e$ where depression dominates (Figure 1C; p=0.45; Student's t-test, two tailed). Thus, PHP is achieved by doubling synaptic vesicle release without altering the expression of STP, confirming prior observations in this system (Weyhersmüller et al., 2011; Müller et al., 2012; Müller et al., 2015; Orr et al., 2017). We sought to understand how this effect could be achieved.

As outlined in the introduction, STP is strongly influenced by the partition of the readily releasable vesicle pool into two functional subclasses: 1) docked vesicles that have a low intrinsic calcium sensitivity of release that are referred to as 'primed' and 2) docked vesicles that have a relatively higher intrinsic calcium sensitivity and are referred to as 'super-primed'. A synapse with a large fraction of super-primed vesicles will show synaptic depression while a synapse with a small number of super-primed vesicles will facilitate. We hypothesize that the ratio of primed to super-primed vesicles is somehow maintained during the expression of PHP, allowing for a dramatic potentiation of vesicle release without altering the dynamics of release during a stimulus train. To test this hypothesis, we used phorbol esters to probe the ratio of primed to super-primed vesicles at the *Drosophila* NMJ.

It is well established that phorbol esters (PdBu) decrease the energy barrier to synaptic vesicle fusion, effectively converting the docked/primed vesicle pool into a super-primed, high release probability state (Lee et al., 2013; Taschenberger et al., 2016). Thus, magnitude of PdBu-dependent potentiation of presynaptic release is proportional to the size of the pool of synaptic vesicles that reside in a docked/primed, but not super-primed state. If PHP-dependent potentiation of presynaptic release preserves the ratio of primed to super-primed vesicles, then the effects of PdBu should be the same prior to and following application of PhTx to the synapse.

We first characterize the use of PdBu at the *Drosophila* NMJ. At 0.75mM $[Ca^{2+}]_e$, PdBu strongly potentiates both evoked and spontaneous vesicle fusion and converts STP from facilitation to depression (Figure 1A, D, E). Specifically, PdBu has no effect on mEPSP amplitude (Figure 1E), causes a significant increase in EPSC amplitude (Figure 1E) and a corresponding increase in quantal content (Figure 1E). We then express the effects of PdBu as a percent change compared to baseline in the absence of PdBu, observing a significant ~140% increase in release (Figure 1E, right; $p<0.05$). Three further effects were also quantified. First, application of PdBu causes a significant decrease in the paired-pulse ratio (Figure 1D; $p<0.05$). Second, we show that presynaptic release converges to a statistically similar steady state in the presence and absence of PdBu during a prolonged stimulus train (Figure 1, figure supplement 1; $p>0.1$, Student's t-test, two-tailed; comparison of final three data points of stimulus train). Third, just as observed at the mammalian central synapses, we demonstrate that the effects of PdBu are dependent on the concentration of

191 extracellular calcium (Lee et al., 2013; Taschenberger et al., 2016). When
192 recording at elevated extracellular calcium (3mM $[Ca^{2+}]_e$), the effect of PdBu on
193 EPSC amplitude is absent (Figure 1F). These data are consistent with the
194 existence of a finite pool of docked vesicles that are uniformly accessed by
195 action-potential induced release at elevated calcium, rendering PdBu without
196 effect. Thus, PdBu functions comparably in Drosophila and at mammalian central
197 synapses. And, by comparing the effects of PdBu on synaptic transmission at
198 0.75mM $[Ca^{2+}]_e$ we can gain an estimate of the fraction of vesicles that exist
199 within the primed versus super-primed state. Specifically, the magnitude of
200 PdBu-mediated potentiation at 0.75mM $[Ca^{2+}]_e$ is proportional to the number of
201 vesicles that remain in the primed (*not* super-primed) state.
202 We next examined the effects of PdBu at synapses previously incubated
203 in PhTx. Once again, at 0.75mM $[Ca^{2+}]_e$, PhTx causes a decrease in mEPSP
204 amplitude, an increase in quantal content and no change in evoked EPSC
205 amplitude (Figure 1E). When PdBu is applied after PhTx, there is no further
206 change in mEPSP amplitude, compared to PhTx alone, as expected (Figure 1E).
207 However, we find that application of PdBu enhances EPSC amplitudes in the
208 presence of PhTx compared to controls with or without PhTx. The consequence
209 is that quantal content is significantly increased compared to PdBu alone and
210 compared to PhTx alone. Indeed, quantal content is potentiated 3-fold compared
211 to baseline release in wild type (from approximately 200 vesicles per action
212 potential to 600 vesicles per action potential). However, when we calculate the
213 percent change in release caused by PdBu compared to PhTx alone, we find that
214 release is potentiated by ~140%, the same percentage increase caused by PdBu

applied to a wild type synapse (Figure 1E). Thus, the proportion of PdBu-sensitive vesicles remains constant following the induction of PHP. Since PHP in a wild type animal can be expressed without a change in short-term plasticity, we propose that the ratio of super-primed to primed vesicles remains constant during expression of PHP (Figure 1G).

Mechanisms that maintain the ratio of primed to super-primed vesicles. We sought to define the underlying molecular mechanisms that might be responsible for maintaining a precise ratio of primed to super-primed vesicles. It is well established that two synaptic proteins, Unc13 and Unc18, participate in the maturation of vesicles from a docked to a primed and, potentially, super-primed state (He et al., 2017; Park et al., 2017; Deak et al., 2009). Recent evidence demonstrates that a mutation that deletes Drosophila *Unc13A* has no effect on the rapid induction of PHP (Martin Mueller personal communication). By contrast, there is prior evidence that Unc18 might participate in the mechanisms of PHP at the rodent NMJ (Sons et al., 2003). Therefore, we focused our attention on Unc18.

Unc-18 is a member of the Sec1/Munc-18 family of syntaxin binding proteins, conserved from yeast to human. Unc-18 is an essential component of the macromolecular synaptic vesicle fusion apparatus. At the neuronal synapse, deletion of the Unc-18 orthologues in worm, fly and mice largely abolish both spontaneous and action potential evoked synaptic vesicle release (Weimer et al., 2003; Harrison et al., 1994; Verhage et al., 2000). But, examination of

heterozygous (*unc-18-1/+*) mutants has provided some interesting insight into the potential function of Unc-18 in homeostatic plasticity.

Synaptic transmission persists at *Drosophila*, mouse and human synapses in a heterozygous (*unc-18-1/+*) mutant background (Wu et al., 1998; Toonen et al., 2006; Patzke et al., 2015). Synaptic efficacy is diminished in these animals, indicating that the levels of Unc-18 are limiting for evoked neurotransmitter release (Patzke et al., 2015; Wu et al., 1998; Toonen et al., 2006). Thus, the heterozygous mutant is a condition amenable to exploring whether Unc-18 is also limiting for presynaptic forms of neural plasticity. At the mouse NMJ, it was previously shown that expression of PHP is suppressed by approximately 25% in the heterozygous *unc-18-1/+* mutant background (Sons et al., 2003). One possibility is that Unc-18-1 represents an evolutionarily conserved interface of homeostatic signaling and the synaptic vesicle fusion apparatus (Sons et al., 2003). However, because diminished levels of Unc-18-1 limit presynaptic release at the mouse NMJ, it is equally plausible that loss of Unc-18 simply restricts the full expression of PHP through a ceiling effect. We sought to use the Drosophila system to further explore the function of Unc18 during PHP and test whether Unc18 is a critical component that stabilizes STP during the induction and expression of PHP.

Rop is required in the rapid induction of presynaptic homeostasis

In *Drosophila*, there is a single neuronally expressed *unc-18* gene, termed *Rop* (***R****as* ***op****posite*). Throughout this paper, from this point onward, we refer to the *Drosophila* gene as *Rop* and orthologues in other species as *unc-18*. Prior

genetic analyses isolated and characterized numerous mutations in the *Rop* gene, demonstrating that Rop is essential for spontaneous and evoked synaptic vesicle fusion, in agreement with data from other species (Harrison et al., 1994; Wu et al., 1998; Toonen and Verhage, 2007). We have taken advantage of previously characterized mutations in *Rop* to study the role of Unc-18 in presynaptic homeostatic plasticity (PHP).

We assayed PHP in two independent, heterozygous *Rop* loss-of-function mutants: 1) a previously characterized null allele (Rop^{G27}; Harrison et al. 1994; see Figure 2A) and 2) a small chromosomal deficiency that deletes the entire *Rop* gene locus ($Df^{(3L)BSC735}$, referred to hereafter as Df^{Rop}; Cook et al. 2012; Figure 2A). In both Rop^{G27}/+ and Df^{Rop}/+ heterozygous mutants, PHP is significantly suppressed compared to wild type (Figure 2B-2I). Specifically, upon application of PhTx, Rop^{G27}/+ mutants show an enhancement of quantal content (Figure 2H; $p<0.01$), but the magnitude of this enhancement is statistically significantly smaller than that observed in wild type (Figure 2I; $p<0.001$). Consistent with impaired homeostatic plasticity, EPSP amplitudes are significantly reduced in the presence of PhTx compared to baseline EPSP amplitudes (Figure 2C and 2G; $p<0.05$; $p<0.0001$). Notably, baseline release, recorded in the absence of PhTx, is unaltered in both Rop^{G27}/+ and Df^{Rop}/+ heterozygous mutants at the concentration of external calcium used in this experiment (0.3 mM $[Ca^{2+}]_e$) (Figure 2C and 2G). Thus, two independently derived heterozygous loss-of-function mutants suppress PHP without an effect on baseline neurotransmission, arguing that PHP is highly sensitive to *Rop* gene dosage.

Neuronally expressed Rop is required for presynaptic homeostasis

The *unc-18* gene is broadly expressed and has been shown to participate in membrane trafficking events outside the nervous system (Hata and Südhof, 1995; Riento et al., 2000; Toonen and Verhage, 2003). As such, Rop could function either pre- or postsynaptically during PHP. Therefore, we knocked down *Rop* expression specifically in the nervous system using the *Gal4/UAS* expression system. We took advantage of a previously characterized *UAS-Rop-RNAi* transgene (*P{GD1523}v19696*; Dietzl et al. 2007) to knock-down *Rop* specifically in neurons (*c155-Gal4*; Lin & Goodman, 1994). First, we demonstrate that PHP is strongly suppressed when *UAS-Rop-RNAi* is driven presynaptically (Figure 3A-E). Thus, Rop is necessary presynaptically for PHP. We note that presynaptic *Rop* knockdown also causes a decrease in baseline EPSP amplitude and quantal content by ~30% (Figure 3C; $p<0.01$), suggesting that presynaptic knockdown depletes Rop protein levels more substantially than that observed in the heterozygous *Rop* null mutant (Figure 2F-I). Indeed, when we compare wild type, Rop^{G27}/+ and presynaptic *Rop* knockdown, we find a progressively more severe decrease in mEPSP frequency that is consistent with progressively more severe depletion of Rop protein (Figure 3F). Thus, *Rop* knockdown can be considered a strong hypomorphic condition, supporting the conclusion that presynaptic Rop is essential for robust expression of PHP.

Separable activity of Rop during baseline transmission and PHP

Although PHP is selectively impaired in the *Rop*^{G27}/+ heterozygous mutant at 0.3mM $[Ca^{2+}]_e$, it remains formally possible that loss of Rop places a limit on the number of vesicles that can be released per action potential (quantal content) and, thereby, indirectly restricts the expression of PHP. To address this possibility, we asked whether baseline release and PHP change in parallel as a function of altered extracellular calcium in the *Rop*^{G27}/+ heterozygous mutations. Experiments were conducted at 0.3mM $[Ca^{2+}]_e$, 0.75 mM $[Ca^{2+}]_e$, 1.5 mM $[Ca^{2+}]_e$ and 3.0 mM $[Ca^{2+}]_e$. First, we find that baseline neurotransmitter release is impaired at 0.75 as well as 1.5 and 3.0 mM $[Ca^{2+}]_e$ in the *Rop*^{G27}/+ heterozygous mutants compared to wild-type (Figure 4). But, there remains a highly cooperative relationship between extracellular calcium and vesicle release in the *Rop*^{G27}/+ heterozygous mutants (Figure 4F). Next, we demonstrate that PHP is suppressed both at 1.5 mM (Figure 4A-C) and 3.0 mM $[Ca^{2+}]_e$ (Figure 4D-E), as evidenced by an inability of EPSCs to be restored to baseline values in the presence of PhTx (Figure 4C and 3E) ($p<0.05$). When we calculate the percent suppression of PHP at 0.3, 1.5, and 3.0 mM $[Ca^{2+}]_e$ we find a constant level of PHP suppression even though baseline release increases ~10-fold over this range of extracellular calcium concentrations (Figure 4F). From this we can make two conclusions. First, since release remains sensitive to changes in external calcium, a ceiling effect cannot explain the defect in PHP observed in the *Rop*^{G27}/+ heterozygous mutants. More specifically, the increase in release in *Rop*^{G27}/+ comparing 0.3 mM $[Ca^{2+}]_e$ with 3.0 mM $[Ca^{2+}]_e$ vastly exceeds the change in vesicular release that would be expected for full expression of PHP at 0.3 mM $[Ca^{2+}]_e$ (see figure 2). The fact that PHP is consistently inhibited by ~30%,

irrespective of the concentration of external calcium, demonstrates that the magnitude of PHP expression correlates directly with the levels of *Rop* expression, not with the magnitude of evoked release or extracellular calcium concentration, arguing for an essential role of Rop in the mechanisms of PHP.

Rop dependent vesicle priming correlates with expression of PHP

Unc-18 has been implicated in several different stages of the release process, including vesicle docking, priming, fusion pore formation and regulation of the readily releasable pool (RRP) of synaptic vesicles (Weimer et al., 2003; Toonen et al., 2006; Gulyás-Kovács et al., 2007; Fisher et al., 2001; Toonen and Verhage, 2007). Since we observe a significant disruption of PHP in the heterozygous Rop^{G27}/+ mutant background, we sought to define the parameters of presynaptic release that are particularly sensitive to the heterozygous Rop^{G27}/+ mutant, highlighting those actions of Rop that best correlate with impaired PHP. First, we observe a decrease in the frequency of spontaneous mEPSP events in *Rop* mutants (Figure 3F). mEPSP frequency is decreased by 36% and 59% compared to wild-type in Rop^{G27}/+ and *UAS-Rop-RNAi,* respectively (Figure 3F). This is consistent with prior reports in *Drosophila* and other systems (Wu et al., 1998; Toonen et al., 2006; Patzke et al., 2015).

It has previously been shown that a homeostatic modulation of the readily releasable pool (RRP) of vesicles is required for the expression of PHP (Müller et al. 2012). RRP size can be estimated through quantification of the cumulative EPSC amplitude during a high frequency stimulus train (60 HZ, 30 stimuli) at elevated extracellular calcium (1.5 mM; Figure 5) and back extrapolation

according to published protocols (Schneggenburger et al. 1999; Müller et al., 2015). We demonstrate that the cumulative EPSC amplitude in the *Rop*^{G27}/+ heterezogous mutant is unaltered at baseline compared to wild-type (Figure 5B). Then, we demonstrate that the *Rop*^{G27}/+ mutants show normal modulation of the RRP following application of PhTx, as demonstrated the maintenance of the cumulative EPSC amplitude in the presence and absence of PhTx, which diminishes the amplitude of underlying unitary release events by ~50% (Figure 5B). Thus, at the *Drosophila* NMJ, the RRP is not sensitive to *Rop* haplo-insufficiency and Rop is not limiting for the homeostatic potentiation of the RRP.

It remains apparent, however, that the initial EPSC of the stimulus train in *Rop*^{G27}/+ mutants, recorded in the presence of PhTx, is smaller than that observed in wild type (Figure 5A-B see also Figure 3C for quantification). Thus, the homeostatic potentiation of the initial EPSC amplitude is disrupted in the *Rop*^{G27}/+ mutants, whereas the homeostatic potentiation of the RRP is normal. This is quantified by dividing the initial EPSC amplitude by the cumulative EPSC amplitude during the stimulus train, a parameter referred to as P_{train} (Figure 5C). It is apparent that release dynamics are altered as a consequence of decreased P_{train} in the *Rop*^{G27}/+ mutant in the presence of PhTx. Super-priming should contribute significantly to vesicle release in response to the first action potential of a stimulus train. Thus, one explanation for this result is that the super-primed vesicle pool has not been appropriately expanded in the *Rop*^{G27}/+ mutant. During the stimulus train, elevated intra-terminal calcium could overcome *Rop*^{G27}/+ haploinsufficiency by driving the normal priming process, leading to expansion of the RRP in the presence of PhTx. These data argue that Rop may be essential

for the expansion of the super-primed vesicle pool during expression of PHP. It is worth noting that this is the first example of a significant alteration in presynaptic release dynamics that is specific to the induction of PHP.

A genetic interaction of Rop and RIM during PHP.

There has been considerable progress identifying presynaptic proteins that are necessary for presynaptic homeostatic plasticity (Davis, 2013; Müller and Davis, 2015). These genes include the active zone associated scaffolding proteins RIM (Rab3 Interacting Molecule) and RBP (RIM Binding Protein), both of which are components of a proposed molecular priming pathway within the presynaptic nerve terminal (Sudhof, 2012). If Rop is integrally involved in the mechanisms of PHP within the presynaptic terminal, potentially acting in the priming process during PHP, then we might expect genetic interactions with *rim* and *RBP*. Genetic interactions were performed by assaying heterozygous, null mutations alone and in comparison to the effects observed in a double heterozygous condition (Frank et al., 2009, Müller et al., 2015). We first assayed baseline release. At 0.3 mM $[Ca^{2+}]_e$, baseline release was normal in both Rop^{G27}/+ and rim^{103}/+ (Figure 6B). However, release (quantal content; 6C) was diminished by nearly 50% in the double heterozygous condition (WT QC = 34.8 ± 0.8; Rop^{G27}/+ QC = 30.1 ± 1.6; rim^{103}/+ QC = 32.3 ± 1.4; Rop^{G27}/ rim^{103} QC= 18.7 ± 1.3) (Figure 6C). This is a very strong genetic interaction for baseline release, even by comparison with previously published genetic interactions of other genes with *rim* (Wang et al. 2016; Orr et al., 2017; Hauswirth et al., 2018).

Next, we assessed PHP. Upon application of PhTx, a heterozygous null mutation in *rim (rim^{103}/+)* causes a suppression of PHP (Figure 6D). This suppression is similar in magnitude to that observed in the *Rop^{G27}*/+ heterozygous null mutation (Figure 6D). However, when we examine a double heterozygous mutant with *Rop^{G27}* /+ placed in trans to *rim^{103}* /+, PHP is completely blocked (Figure 6C, D). To underscore the robustness of this genetic interaction, we plot the relationship between mEPSP amplitude and quantal content for individual recordings (Figure 6E). Each data point represents the average mEPSP and quantal content for a single NMJ recording (see also Hauswirth et al., 2018). In wild type, data can be fit with a line representing the homeostatic process. We also present dotted lines that encompass 95% of all of the data points in the wild type graph. This fit and 95% data interval are used to compare data distributions to other mutant background. In both of the single heterozygous mutants (*Rop^{G27}* /+ and *rim^{103}* /+) the data points lie below the best-fit line for wild type, but are largely retained within the 95% interval, consistent with a minor suppression of PHP when all data points are averaged (Figure 6C, D). However, in the double heterozygous animal (*Rop^{G27} / rim^{103}*) it is clear that PHP fails and the majority of data points in the presence of PhTx reside outside the interval that contains 95% of all wild type data points. More specifically, for heterozygous null *Rop* and *rim* recordings in the presence of PhTx, 25% and 16% of these individual data points in the presence of PhTx fall outside of the lines encompassing 95% of wild-type data (Figure 6E). In the double heterozygous mutants, 87% of PhTx data fall outside of the 95% confidence intervals (Figure 6E). This genetic interaction, referring specifically to PHP

428 expression, is also conserved at elevated calcium levels (1.5 and 3.0 mM
429 calcium; data not shown).
430 At baseline, there is a strong synergistic interaction between Rop and
431 RIM, suggesting that both are functioning to control the same process relevant to
432 vesicle release, perhaps synaptic vesicle priming (Gulyás-Kovács et al., 2007;
433 Koushika et al., 2001). It remains unclear whether *rop* and *rim* function in the
434 same genetic pathway based on this genetic interaction. The data are equally
435 compatible with parallel pathways converging on the mechanism of PHP.
436 Regardless, our data underscore that Rop has an essential function during the
437 process of PHP. We consider this a particularly important line of reasoning,
438 since it is not feasible to eliminate *Rop* and assess a block in PHP.
439 Next, we sought to understand the specificity of the genetic interaction
440 between *Rop* and *rim*. To do so, we performed a series of additional genetic
441 interactions with other genes previously implicated in the presynaptic synaptic
442 vesicle priming process. First, we asked whether *Rop* shows a genetic interaction
443 with *RIM Binding Protein (RBP)*. RBP biochemically interacts with RIM and is
444 thought to form an extended presynaptic scaffold (Wang et al., 2000; Liu et al.,
445 2011). In *Drosophila*, RBP is also essential for both baseline release and PHP
446 (Müller et al., 2015). But, the mechanism by which RBP participates in PHP is
447 distinct from the mechanism by which RIM participates in PHP (Müller et al.,
448 2015). The heterozygous null mutation in *rbp*/+ has no effect on baseline
449 transmission at 0.3mM external calcium, consistent with prior observations
450 (Müller et al., 2015) (Table 1). We then demonstrate that PHP is also normal in
451 the Rop^{G27}/ rbp^{STOP1} double heterozygous mutant (Figure 6F). This is evidence

that there is specificity to the *rop* interaction with *rim* during PHP. It is worth noting that PHP is highly variable in the Rop^{G27}/ rbp^{STOP1} double heterozygous mutant, preventing us from making any additional conclusions regarding whether PHP is similar to, or different from wild type.

Next, we asked whether *rim* genetically interacts with *Unc-13* during baseline neurotransmitter release and PHP. Munc-13 is known to biochemically interact with RIM (Betz et al., 2001). Alone, the $dunc\text{-}13^{P84200}$/+ heterozygous null mutation has no effect on baseline transmission or PHP (Table 1). Remarkably, the double heterozygous condition of *rim* and *dunc-13* also has no effect on baseline transmission or PHP (Table 1 and Figure 6G). A similar set of findings is observed when we tested a double heterozygous condition of *rim* with *rbp* (Table 1 and Figure 6H). While baseline transmission is decreased in the double heterozygous combination of *rim*/+ and *rbp*/+, we find that PHP is normal, confirming previously published data (Müller et al., 2015). It is somewhat surprising that the *rim*/+ ; *unc13*/+ double heterozygous mutant has significantly more PHP than observed in *rim*/+ alone, perhaps relating to the functional importance of the RIM-Unc13 biochemical interaction during PHP. Regardless, when taken together, our results underscore the specificity and importance of the genetic interaction between *rop* and *rim* and the relevance of *rop* to the mechanisms of PHP.

Loss of Rop and Rim limits the super-primed vesicle pool

We note that heterozygous Rop^{G27}/+ mutants have a defect in PHP that is apparent on the first action potential of a stimulus train, but the homeostatic

476 expansion of the RRP is apparent upon further stimulation (Figure 5). Both Rop
477 and Rim are well-established molecular players that contribute to synaptic vesicle
478 priming (Sudhof, 2012a,b). We returned to the use of PdBu to assess whether
479 the block of PHP in the *Rop^{G27}/rim^{103}* double heterozygous mutant is correlated
480 with a deficit in vesicle super-priming. As outlined above, the magnitude of PdBu-
481 dependent potentiation in response to a single action potential should reflect the
482 balance of primed to super-primed vesicles. A large PdBu effect argues for a
483 smaller pool of super-primed vesicle pool. We compared wild type to the
484 *Rop^{G27}/rim^{103}* double heterozygous mutant, recording in the presence and
485 absence of PdBu (Figure 7). Experiments were performed at 0.75mM $[Ca^{2+}]_e$, a
486 condition in which PdBu potentiates wild type synapses by ~165% (Figure 7A-D).
487 Next, we demonstrate that application of PdBu to each heterozygous mutant
488 alone, either *Rop^{G27}*/+ or *rim^{103}*/+, is identical to wild type (Figure 7C,D; p>0.1
489 ANOVA). Then, we demonstrate that PdBu has a dramatically increased effect
490 size when applied to the *Rop^{G27}/rim^{103}* double heterozygous mutant, potentiating
491 release by more than 350%, a dramatically increased effect size compared to
492 application of PdBu to wild type and single heterozygous controls (Figure 7A-D,
493 p<0.01; ANOVA). These data argue that the *Rop^{G27} /rim^{103}* double heterozygous
494 mutant limits the size of the super-primed vesicle pool, thereby impairing vesicle
495 release in response to a single action potential, an effect that is strongly
496 correlated with a block in the expression of PHP. Two other observations should
497 be noted. First, the *Rop^{G27}/rim^{103}* double heterozygous mutant recorded at
498 0.75mM $[Ca^{2+}]_e$ has a greater effect on baseline release than observed at 0.3mM
499 $[Ca^{2+}]_e$. The basis for this effect is unknown. Second, we show that the enhanced

effects of PdBu on the *Rop*^{G27}/ *rim*^{103} double heterozygous mutant is consistent with the potentiation of release probability and an associated change in paired pulse ratio (Figure 7C). This simply confirms that PdBu is behaving as expected when applied to the *Rop*^{G27}/*rim*^{103} double heterozygous mutant. Again, this type of synergistic genetic interaction is generally taken as evidence that two genes participate in the same process. It is not possible to make any conclusion regarding whether these genes are acting in a linear signaling pathway or in parallel signaling pathways. But, based on formal genetic argument, we are able to conclude that they likely converge to control the same processes at the presynaptic terminal, both the PdBu sensitive vesicle pool and PHP.

Loss of *syx1A* rescues PHP in the heterozygous *rop* mutant background

Unc-18 is a well-established syntaxin binding protein (Hata et al., 1993; Pevsner et al., 1994; Halachmi et al., 1995). The Unc-18 interaction with Syntaxin is complex, including progressive interactions with closed and open conformations of Syntaxin. Ultimately, the Unc-18 interaction with open Syntaxin is thought to catalyze SNARE assembly, greatly decreasing the energy barrier to calcium-driven vesicle fusion. Indeed, Unc-18 binding to open Syntaxin is believed to be a prerequisite for efficient synaptic vesicle fusion (Dulubova et al., 2007; Deák et al., 2009). Based on the genetic interactions reported above, we expected that loss of *syx1A* would strongly enhance the loss of function phenotype of the heterozygous *Rop*^{G27}/+ mutant, resulting in diminished vesicle release and a block of PHP.

We acquired a previously published null mutation in *syntaxin1A* and examined baseline neurotransmitter release in a heterozygous *syx1A* mutant (*syx1A*$^{\Delta 229}$*;* Schulze et al. 1995). There is no change in baseline mEPSP amplitude, EPSP amplitude or quantal content in *syx1A*$^{\Delta 229}$/+ assayed at 0.3mM $[Ca^{2+}]_e$ (Figure 8A-D). Thus, *syntaxin* is not haplo-insufficient for baseline release. Remarkably, the same is true for the double heterozygous condition, combining *syx1A*$^{\Delta 229}$/+ with *Rop*^{G27}/+. Baseline transmission is normal compared to wild type (Figure 8D). In other systems, it is estimated that Syntaxin1A is present in ~5-fold excess compared to the levels of synaptic Unc-18 (Graham et al., 2004). This could explain the lack of a genetic interaction at baseline.

Next, we examined PHP. A heterozygous null mutation in *syx1A* (*syx1A*$^{\Delta 229}$/+) has normal PHP (Figure 8E), again consistent with a possible excess of Syntaxin protein at the release site. The heterozygous null mutation in *Rop* (*Rop*^{G27}/+) suppresses homeostatic potentiation (Figure 8E), confirming experiments presented earlier in this study. Remarkably, when we place *Rop*^{G27} in *trans* to *syx1A*$^{\Delta 229}$ (double heterozygous condition), we find that homeostasis is fully expressed (Figure 8E). Impaired PHP caused by the *Rop*^{G27}/+ mutation is completely rescued to wild type levels. More specifically, in the double heterozygous mutants, EPSP amplitudes fully compensate in the presence of PhTx (Figure 8C) and there is a wild type level enhancement of quantal content (Figure 8E) in the presence of PhTx. Finally, the rescue of the *Rop*^{G27}/+ mutation by *syx1A*$^{\Delta 229}$/+ is not restricted to PHP. The rate of spontaneous vesicle fusion is also restored to wild type levels, underscoring the validity of this genetic rescue (Figure 8F). Note that there is, as yet, no indication that mEPSP frequency is

directly responsible for the induction of PHP (Frank et al., 2006, 2009; Harris et al., 2015; Goold and Davis, 2007). Since we are examining heterozygous, null mutations, the most parsimonious conclusion is that Syntaxin normally functions to restrict the action of Rop that is required for PHP. Reducing the level of Syntaxin relieves a restriction on Rop activity and restores full expression of PHP. To provide further evidence for this surprising finding, we sought to disrupt the physical interaction of Rop and Syntaxin and assess whether this might also rescue the expression of PHP in the Rop^{G27}/+ mutant background.

Evidence that Syx1A restrains Rop from participating in PHP

We performed an *in vitro* binding assay to confirm the biochemical interaction between Rop and Syntaxin1A. Recombinant wild-type Rop protein binds strongly to recombinant Syntaxin1A (GST-syx1A$^{\Delta C}$) (Figure 9B-C) (K_D=0.4μM). Next, we surveyed previously characterized point mutations in the *Rop* gene, searching for candidate mutations that reside near the conserved Syntaxin binding interface (Figure 9A). Unc-18 binds to Syntaxin at two sites, an N-terminal region that interacts with the N-terminal peptide of Syntaxin and a helical region that represents a larger interaction surface. The Rop^{G11} mutant harbors a point mutation (Asp 45→ Asn; Harrison et al. 1994) that resides within or directly adjacent to a predicted helical Syntaxin binding interface (Misura et al. 2000). Here, we demonstrate that this mutation completely abolishes *in vitro* binding between recombinant Rop^{G11} mutant protein and recombinant GST-syx1A$^{\Delta C}$ protein (Figure 9B-C) (K_D=36.1μM).

570 We next assayed baseline release in the *Rop*^{G11} mutant, placed in trans to
571 either a deficiency that removes the *Rop* gene locus, or the *Rop*^{G27} null allele. To
572 our surprise, both allelic combinations are viable to the third instar stage and we
573 observe robust neurotransmitter release (Figure 9D). Specifically, we find that
574 EPSC amplitudes are decreased by ~45% on average in both the *Rop*^{G11}/*Df*^{Rop}
575 and *Rop*^{G11}/*Rop*^{G27} allelic combinations compared to wild type (*WT*
576 EPSC=217.4nA ± 7.3; *Rop*^{G27}/*Rop*^{G11} EPSC=134.2nA ± 12.2; p<0.01;
577 *Df*^{Rop}/*Rop*^{G11} EPSC=156.3nA ± 17.2; p<0.01) (Figure 9F). This effect is more
578 severe than the defect observed in the *Rop*^{G11}/+ heterozygous condition,
579 consistent with loss of Rop function in both the *Rop*^{G11}/ *Df*^{Rop} and *Rop*^{G11}/*Rop*^{G27}
580 allelic combinations. But, the presence of synchronous release is very surprising,
581 since there is no wild type Rop protein at the synapse. From these data we
582 conclude that the *Rop*^{G11} mutation does not completely block all interactions
583 between Rop and Syntaxin *in vivo*. The *in vitro* binding assay is predicted to test
584 the binding of Rop to the closed conformation of Syntaxin. We speculate, based
585 on work in other systems, that Rop^{G11} could be localized to the SNARE complex
586 through other molecular interactions, *in vivo*. Once at the release site, Rop^{G11}
587 mutant protein might still interact with the open conformation of Syntaxin and
588 facilitate SNARE-mediated fusion.
589 Next, we assayed PHP in the *Rop*^{G11}/+ as well as the *Rop*^{G11}/*Df*^{Rop} and
590 *Rop*^{G11}/*Rop*^{G27} allelic combinations. In the presence of PhTx, EPSC amplitudes
591 are restored to baseline values in the *Rop*^{G11}/+ mutant, indicative of fully
592 functional PHP (Figure 9D-F). Remarkably, PHP is also fully expressed in both
593 the *Rop*^{G11}/*Df*^{Rop} and *Rop*^{G11}/*Rop*^{G27} allelic combinations (Figure 9D-F). Thus, the

presence of the Rop^{G11} allele fully rescues PHP in the presence of the Rop^{G27}/+ as well as the Df^{Rop}/+ alleles. While surprising, these data are entirely consistent with the observation that a heterozygous null mutation in *syntaxin1A* rescues PHP in the Rop^{G27} mutant background (Figure 8). Taken together, our data are consistent with an emerging model in which Syx1A regulates the availability of Rop to participate in PHP (see discussion).

DISCUSSION

We have advanced our understanding of presynaptic homeostatic plasticity in several important ways. First, we demonstrate that *rop* (*Unc-18*) is essential for PHP, significantly extending prior evidence presented at the mouse NMJ (Sons et al., 2003). Thus, we argue that *rop* (*Unc-18*) is an evolutionarily conserved component of PHP signaling, enabling expression of PHP at the NMJ of Drosophila (this paper) and mice (Sons et al., 2003). Indeed, Unc-18 is the first molecular signaling component demonstrated to have a conserved, required function during PHP in both systems. Fly and mouse are separated by nearly 500 million years of evolution, suggesting that the molecular mechanisms of PHP may be as ancient as mechanisms that achieve action-potential induced, calcium-dependent, neurotransmitter release.

Second, our data demonstrate that Rop is limiting for the expression of PHP. Prior work at the mouse NMJ was the first to provide evidence that Unc-18 might participate in PHP (Sons et al., 2003). However, the prior work only included an analysis of *Unc-18*/+ heterozygous null mutant animals and, ultimately, could not rule out the formal possibility that Unc-18 was essential for

baseline release and, as a secondary consequence, limited the expression of PHP. We provide several lines of evidence supporting the conclusion that Unc-18 has an activity that is necessary for PHP. For example, neurotransmitter release in the heterozygous Rop^{G27} /+ mutant remains highly sensitive to changes in extracellular calcium. Yet, across a 10-fold range of extracellular calcium, PHP is suppressed by a constant fraction of ~30%. We also pursued a series of genetic interactions and provide evidence for a strong, specific, genetic interaction of *Rop* with *rim*, placing Unc-18 within a known PHP signaling framework.

Third, Unc-18 is the first integral component of the synaptic vesicle fusion apparatus to be linked to the expression of PHP. As such, our data provide a reasonable endpoint for the presynaptic homeostatic signaling system. In recent years, trans-synaptic signaling molecules have been shown to be required for PHP including Semaphorin/Plexin signaling (Orr et al., 2017), innate immune signaling (Harris et al., 2015) and signaling from the synaptic matrix (Wang et al., 2016). Many of these signaling systems interact with the presynaptic scaffolding protein RIM (Harris et al., 2015; Wang et al. 2016; Orr et al., 2017; Hauswirth et al., 2018). But, it was previously unknown what molecular mechanisms reside downstream of RIM, since RIM is a molecular scaffolding protein. We cannot formally conclude, based on our genetic data, that Rop functions downstream of RIM. However, it is clear that Rop is in a position to directly modulate the fusion apparatus and, as such, is very likely to mediate signaling that is localized to the active zone by the RIM-dependent cytomatrix.

The rescue of PHP by loss of Syntaxin or by disruption of Rop-Syntaxin binding is a surprise, but one that can be understood when placed in the context

642 of work previously documented in other systems. A recent single molecule
643 imaging study demonstrates that the majority of Unc-18 may reside outside of
644 active zone with limited mobility (Smyth et al., 2013). It has also been shown that
645 Syntaxin is present in large excess compared to Unc-18, and Syntaxin protein is
646 broadly distributed beyond sites of synaptic vesicle fusion (Broadie et al., 1995;
647 Graham et al., 2004). Thus, the majority of Unc-18 protein could interact with
648 Syntaxin in the peri-active zone, presumably binding a closed Syntaxin
649 conformation. Accordingly, Unc-18 would be in equilibrium, moving between a
650 peri-active zone reservoir and fusion competent vesicles at the active zone. In
651 this way, Syntaxin could restrict the amount of Unc18 available for participation in
652 synaptic vesicle fusion at the release site. Thus, when we remove one copy of
653 the *syntaxin* gene, or diminish the binding of Unc-18 to the closed confirmation of
654 Syntaxin, we might be shifting the distribution of Unc-18 toward the release site
655 and achieve a rescue PHP. This model is consistent with data in other systems,
656 demonstrating that the levels of Unc18 at the release site can influence vesicle
657 release rate. For example, over-expression of *unc-18* in mice is sufficient to
658 potentiate vesicle release (Voets et al., 2001), albeit to a limited extent (Toonen
659 and Verhage, 2003). Thus, we propose that the expression of PHP involves an
660 as yet unknown signaling event that mobilizes Unc-18 to the active zone where it
661 is sufficient to promote vesicle priming as a final stage necessary for the full
662 expression of PHP.
663
664 **PHP potentiates release without altering release dynamics.**

665 Homeostatic signaling systems are powerful corrective processes. One of the
666 most remarkable properties of PHP is that synaptic gain is controlled without
667 altering presynaptic release dynamics (Figure 1). The expression of PHP
668 includes a required potentiation of presynaptic calcium influx (Müller and Davis,
669 2012), a required expansion of the readily releasable synaptic vesicle pool
670 (Müller et al., 2012; Müller et al., 2015) and, as demonstrated here, increased
671 function of Unc-18 dependent vesicle priming. Only when all three processes are
672 simultaneously potentiated is it possible to achieve increased presynaptic release
673 while precisely preserving presynaptic release dynamics. The capacity to sustain
674 release dynamics underscores the emerging molecular complexity of PHP
675 signaling. Each of the three processes that control release are under homeostatic
676 control. A PHP-dependent change in calcium influx is controlled by ENaC
677 channel insertion (Younger et al., 2013). The PHP-dependent modulation of the
678 RRP involves signals converging on the synaptic cytomatrix including RIM, RBP
679 and regulation of presynaptic actin (Müller et al., 2012; Müller et al., 2015; Orr et
680 al., 2017). Future work will be necessary to establish the inter-dependence of
681 these presynaptic homeostatic signaling pathways.

682 Here, we present evidence that one function of Unc18 may be to ensure
683 that the ratio of primed to super-primed vesicles remains constant during the
684 doubling of presynaptic release occurring during PHP. Several lines of evidence
685 support this conclusion. PHP is fully expressed following single action potential
686 stimulation, necessitating expansion of the docked/primed vesicle pool. We use
687 PdBu to determine the fraction of docked/primed vesicles that reside in the
688 super-primed state versus a lower-release probability docked/primed stated. We

689 find that the ratio of primed to super-primed vesicles remains constant during
690 PHP. When PdBu is applied to the NMJ, converting the entire pool to a super-
691 primed state, release dynamics are converted to synaptic depression, arguing
692 that preservation of the primed to super-primed ratio is essential for maintaining
693 wild type release dynamics. Then, two results connect Unc18 function to control
694 of the super-primed pool. First, loss of Rop (Unc18) primarily affects the first
695 EPSC of a stimulus train, consistent with control of the super-primed vesicle pool.
696 Second, when Rop^{G27}/+ is combined with rim^{103}/+, the double heterozygous
697 condition completely blocks PHP expression and there is a dramatic loss of the
698 super-primed population of vesicles, as revealed by a ~300% increase in the
699 effect of PdBu on presynaptic release.
700 The preservation of presynaptic release dynamics during PHP seems to
701 be a fundamental property of PHP. Not only is synaptic gain stabilized, but also
702 the dynamic, activity-dependent transfer of information at a synapse is precisely
703 preserved. At the neuromuscular junction, the impact is presumably to maintain
704 the quality of muscle excitation. If extended to the central nervous system, where
705 PHP is also observed (Davis, 2013), preservation of release dynamics would
706 stabilize the flow of information through complex neural circuitry, with obvious
707 relevance to processes such as sensory-motor integration and other neural
708 computations. Clearly, many processes must be coordinately controlled by the
709 intracellular signaling systems that participate in presynaptic homeostatic
710 plasticity in order to double vesicular release, at a constant number of active
711 zones, while precisely preserving presynaptic release dynamics. Here, we
712 identify a novel mechanism that participates in PHP and the preservation of

presynaptic release dynamics, the regulated action of Unc18 at the presynaptic release site. This is an important advance toward what must become a systems biology level solution to regulation of presynaptic neurotransmitter release during PHP at central and peripheral synapses.

METHODS

Key Resources Table (see next page)

Reagent type (species) or resource	Designation	Source or reference	Identifiers	Additional information
Gene *(Drosophila melanogaster)*	*Rop*	NA	FLYB: FBgn0004574	
Gene *(D. melanogaster)*	*Rim*	NA	FLYB: FBgn0053547	
Gene *(D. melanogaster)*	*Rbp*	NA	FLYB: FBgn0262483	
Gene *(D. melanogaster)*	*unc-13*	NA	FLYB: FBgn0025726	
Gene *(D. melanogaster)*	*Syx1A*	NA	FLYB: FBgn0013343	
Strain - strain background	WT - w^{1118}	NA	w^{1118}	
Genetic reagent *(D. melanogaster)*	Rop^{G27}	Bloomington Drosophila Stock Center	BDSC: 4381 FLYB FBst0004381 RRID: DGGR_107715	Flybase symbol: bw[1]; Rop[G27] st[1]/TM6B, Tb[+]
Genetic reagent *(D. melanogaster)*	Df^{Rop} *(Df(3L)BSC735)*	Bloomington Drosophila Stock Center	BDSC: 26833 FLYB FBst0026833 RRID: BDSC_26833	Flybase symbol: w[1118]; Df(3L)BSC735/TM6C, Sb[1] cu[1]
Genetic reagent *(D. melanogaster)*	$elav^{C155}$*-GAL4*	Bloomington Drosophila Stock Center	BDSC: 458 FLYB FBst0000458 RRID: BDSC_458	Flybase symbol: P{w[+mW.hs]=GawB}elav[C155]
Genetic reagent *(D. melanogaster)*	*UAS-Rop RNAi*	Vienna Drosophila RNAi Center	VDRC: 19696 FLYB FBst0453580 RRID: FlyBase_FBst0453580	Flybase symbol: w[1118]; P{GD1523}v19696/TM3
Genetic reagent *(D. melanogaster)*	rim^{103}*; rim*	(Müller et al., 2012) PMID: 23175813		
Genetic reagent *(D. melanogaster)*	rbp^{STOP1}	(Liu et al., 2011) PMID: 22174254		gift from Stephan Sigrist
Genetic reagent *(D. melanogaster)*	$dunc\text{-}13^{P84200}$	Kyoto Stock Center	KSC: 101911 RRID: DGGR_101911	Flybase symbol: ry[506] ; P{ry11}l(4)ry16[1] / ci[D]
Genetic reagent *(D. melanogaster)*	$syx1A^{\Delta 229}$	Kyoto Stock Center	KSC: 107713 RRID: DGGR_107713	Flybase symbol: Syx1A[Delta229] ry[506]/TM3, ry[RK] Sb[1] Ser[1]
Genetic reagent *(D. melanogaster)*	Rop^{G11}	(Harrison et al., 1994)		gift from Hugo Bellen

		PMID: 7917291		
recombinant DNA reagent	PMAL-c5E (vector)	New England Biolabs	NEB: N8110	
recombinant DNA reagent	PGEX-4T1 (vector)	Addgene	27-4580-01	
recombinant DNA reagent	Rop (cDNA)	Drosophila Genomics Resource Center	DGRC: SD04216	
recombinant DNA reagent	Syx1A (cDNA)	Drosophila Genomics Resource Center	DGRC: LD43943	
recombinant DNA reagent	PMAL-Rop^{WT} (plasmid)	This paper		Primers CGCGGATCCATGGCCTTGAAAGTGCT GGTGG and CCGGAATTCTTAGTCCTCCTTCGAGAG ACTGC were used to amplify Rop, which was then cloned into PMAL-5ce vector
recombinant DNA reagent	PMAL-Rop^{G11} (plasmid)	This paper		Generated using site-directed mutageneis with primer GGCGGGTGCTGGTGGTGAACAAGCTG GGTATGCGC
recombinant DNA reagent	PGEX-Syx1A$^{\Delta C}$ (plasmid)	This paper		Primers CGCGGATCCATGACTAAAGACAGATT AGCCG and TCCCCCGGGTTACATGAAATAACTGCT AACAT were used to amplify Syx1A, which was then cloned into PGEX-4T1, site-directed mutagenesis with primer GTAAAGCCCGACGAAAGTAGATCATG ATACTGATC was used to remove the C-terminal tail
peptide, recombinant protein	MBP-Rop^{WT}/MBP-Rop^{G11}	This paper		Recombinant MBP-Rop was expressed from PMAL-Rop in Rosetta^{TM} cells, purified using amylose resin, and eluted with maltose
peptide, recombinant protein	GST-Syx1A$^{\Delta C}$	This paper		Recombinant GST-Syx1A$^{\Delta C}$ was expressed from PGEX-Syx1A$^{\Delta C}$ in Rosetta^{TM}, purified using GST resin, and eluted with glutathione
commercial assay or kit	QuikChange Lightning Site-Directed Mutagenesis Kit	Agilent	210518	
commercial assay or kit	Coomassie Blue R-250	TekNova	C1050	

	Solution			
chemical compound, drug	Phorbol 12-myristate 13-acetate Phorbol Ester (PdBU)	Sigma-Aldrich	Sigma-Aldrich CAS: 16561-29-8	Stock concentration: 10 mM Final Concentration (in HL3 saline): 1 µM
chemical compound, drug	Philanthotoxin-433 (PhTX)	Sigma-Aldrich (disc.) Santa Cruz Biotech.	Sigma Aldrich CAS: 276684-27-6 Santa Cruz Biotech. sc-255421	Stock concentration: 5 mM Final Concentration (in HL3 saline): 10-20 µM
software, algorithm	Sharp-electrode recordings	Molecular Devices	Clampex (10.3.1.5)	
software, algorithm	EPSP analysis	Molecular Devices	Clampfit (10.3.1.5)	
software, algorithm	EPSC and Pr analysis	Wave-Metrics	Igor Pro (6.3.4.1) RRID: SCR_000325	custom script
software, algorithm	RRP, train analysis	(Müller et al., 2015)		
software, algorithm	mEPSP analysis	Synaptosoft	Mini Analysis 6.0.7 RRID: SCR_002184	
software, algorithm	GraphPad Prism (7.0c)	GraphPad	RRID: SCR_002798	
software, algorithm	Fiji	NIH	RRID: SCR_002285	
other	Amylose Resin	New England Biolabs	NEB: E8021	used to purify MBP recombinant protein
other	GST Bind Resin	Novagen	70541	used to purify GST recombinant protein and for pull-down of recombinant protein

Fly stocks and Genetics

In all experiments, the w^{1118} strain was used as the wild-type control. Animals were raised between 22-25°C. Rop^{G27} (Harrison et al. 1994), $syx1A^{\Delta 229}$ (Schulze et al. 1995), $dunc\text{-}13^{P84200}$ (Aravamudan et al., 1999), and *Df(3L)BSC735* (Cook et al. 2012) were obtained from the Bloomington Drosophila Stock Center. Rop^{G11} (Harrison et al. 1994) was provided by Hugo Bellen. Rbp^{STOP1} (Liu et al.,

2011) was provided by Stephan Sigrist. *rim*^{103} was generated in the Davis lab as described previously (Müller et al. 2012). *UAS-Rop-RNAi* animals were obtained from Vienna Drosophila Resource Center (VDRC) (stock GD1523). The *elav*^{C155}-*Gal4* driver has been previously described (Lin & Goodman, 1994).

Electrophysiology

Sharp-electrode recordings were made from muscle 6 in abdominal segments 2 and 3 from third-instar larvae using an Axoclamp 2B or Multiclamp 700B amplifier (Molecular Devices), as described previously (Müller et al., 2012). Two-electrode voltage clamp recordings were performed with an Axoclamp 2B amplifier. Recordings were made in HL3 saline containing the following components (in mM): 70 NaCl, 5 KCl, 10 MgCl2, 10 NaHCO3, 115 sucrose, 4.2 trehalose, 5 HEPES, and 0.3 CaCl2 (unless otherwise specified). For acute pharmacological homeostatic challenge, larvae were incubated in Philanthotoxin-433 (PhTX; 10-20 uM; Sigma- Aldrich or Santa Cruz Biotechnology) for 10 min (Frank et al., 2006). EGTA-AM (25 uM in HL3; Invitrogen) was applied to the dissected preparation for 10 min. Recordings were excluded if the resting membrane potential (RMP) was more depolarized than -55mV. A threshold 40% decrease in mEPSP amplitude, below average baseline, was used to confirm the activity of PhTX. After EGTA application, the preparation was washed with HL3. PdBU (1 uM) was applied to the dissected preparation and incubated for 10 min. before recording. Quantal content was estimated by calculating the ratio of EPSP amplitude/average mEPSP amplitude and then averaging recordings across all NMJs for a given genotype. EPSC data were analyzed identically. Paired pulse

752 ratios were quantified by calculating the ratio of the 2nd EPSC/1st EPSC. EPSP
753 and mEPSP traces were analyzed in IGOR Pro (Wave-Metrics) and MiniAnalysis
754 (Synaptosoft).
755 The RRP was estimated by cumulative EPSC analysis (Schneggenburger
756 et al., 1999; Weyhersmüller et al., 2011; Müller et al., 2012). Muscles were
757 clamped at −65 mV in two-electrode voltage configuration, and EPSC amplitudes
758 during a stimulus train (60 Hz, 30 stimuli) were calculated as the difference
759 between peak and baseline before stimulus onset of a given EPSC. The average
760 cumulative EPSC amplitude for a given muscle was obtained by back-
761 extrapolating a line fit to the linear phase (the last 200 ms) of the cumulative
762 EPSC plot to time 0. The apparent RRP size was obtained by dividing the
763 cumulative EPSC amplitude by the mean mEPSP amplitude recorded in the
764 same cell in current clamp mode before placing the second electrode in the
765 muscle.
766
767 **Molecular Biology**
768 The *PGEX-syx1A*$^{\Delta C}$ construct was generated by PCR introduction of
769 BAMHI/SMAI sites at the 5' and 3' ends of *syx1A* cDNA obtained from the
770 Drosophila Genomics Resource Center (DGRC; Source cDNA: LD43943). The
771 BAMHI-SMAI *syx1A* cDNA fragment was then cloned into the *PGEX-4T1* vector
772 (Addgene) by standard techniques to make *PGEX-syx1A*. To remove the C-
773 terminal membrane-bound tail of *syx1A,* the *syx1A* point mutation (A802T) was
774 made by site-directed mutagenesis of *PGEX-syx1A*.
775

776 The *PMAL-Rop* construct was generated by PCR introduction of BAMHI/ECORI
777 sites at the 5' and 3' ends of *Rop* cDNA obtained from the Drosophila Genomics
778 Resource Center (DGRC; Source cDNA: SD04216). The BAMHI-ECORI *Rop*
779 cDNA fragment was then cloned into the PMAL-c5e vector (New England
780 Biolabs) to create *PMAL-Rop*. To generate the *PMAL-Rop*^{G11} construct, the *Rop*
781 point mutation (G133A) was made by site-directed mutagenesis of *PMAL-Rop.*
782 All site-directed mutagenesis reactions were performed using the QuikChange
783 Lightning Site-Directed Mutagenesis Kit (Agilent).
784
785 **Recombinant protein expression and purification**
786 Recombinant MBP-Rop, MBP-Rop^{G11} (D45N) and GST-syx1A$^{\Delta C}$ (amino acids 1-
787 268) were expressed from respective expression vectors *PMAL-Rop, PMAL-*
788 *Rop*^{G11}, and *PGEX-syx1A*$^{\Delta C}$ in Rosetta^{TM} cells (Novagen). Cell pellets were lysed
789 in column buffer (20 mM Tris (pH 7.0), 150 mM NaCl, 2 mM EDTA and 0.1%
790 NP40) and cleared by centrifugation. MBP protein was purified using amylose
791 resin (NEB). GST protein was purified using GST bind resin (Novagen).
792 Proteins were eluted using maltose (for MBP proteins) or glutathione (for GST
793 proteins) per the manufacturers recommendations.
794
795 **In vitro Binding Assay**
796 GST- syx1A$^{\Delta C}$ (2 ug) proteins were bound to GST bind resin (Novagen) for 1
797 hour at 4°C with varying concentrations of MBP-Rop and MBP-Rop^{G11} (uM): 0,
798 0.1, 0.2, 0.3, 0.4, 0.6, 0.8, 1, 1.5, 3, 6, and NP40 buffer (6mM Na2HPO4, 4mM
799 NaH2PO4, 1% NONIDET P-40, 150mM NaCl, 2mM EDTA, 50mM NaF, 4ug/ml

leupeptin, 0.1mM Na3VO4). After washing coated beads in NP40 buffer, proteins were eluted by boiling in 5X SDS sample buffer and denatured by boiling for 10 min. Proteins were resolved by SDS-PAGE on a 4-12% Bis-Tris gel (Life Technologies), stained with Coomassie Blue (TekNova) for 30 minutes and de-stained with destaining solution (50% H_2O, 40% MeOH, 10% Acetic Acid) for 2 hours. The gel analysis tool on Image J was used to quantify the fraction of Rop protein binding to syx1A. The Kd was derived from a dose response curve that was fit to the data using Prism 6.

ACKNOWLEDGEMENTS:

We thank Dr. Ting Ting Wang for critical reading of the manuscript. Supported by NIH Grant R35NS097212 to GWD. We also acknowledge support of the Kavli Institute for Fundamental Neuroscience at UCSF.

REFERENCES

Aravamudan, B., Fergestad, T., Davis, W.S., Rodesch, C.K., and Broadie, K. (1999). Drosophila UNC-13 is essential for synaptic transmission. Nat. Neurosci. *2*, 965–971.

Betz, A., Thakur, P., Junge, H.J., Ashery, U., Rhee, J.S., Scheuss, V., Rosenmund, C., Rettig, J., and Brose, N. (2001). Functional interaction of the active zone proteins Munc13-1 and RIM1 in synaptic vesicle priming. Neuron *30*, 183–196.

Broadie, K., Prokop, A., Bellen, H.J., O'Kane, C.J., Schulze, K.L., and Sweeney, S.T. (1995). Syntaxin and synaptobrevin function downstream of vesicle docking in Drosophila. Neuron *15*, 663–673.

Burrone, J., O'Byrne, M., and Murthy, V.N. (2002). Multiple forms of synaptic plasticity triggered by selective suppression of activity in individual neurons. Nature *420*, 414–418.

Cook, R.K., Christensen, S.J., Deal, J.A., Coburn, R.A., Deal, M.E., Gresens, J.M., Kaufman, T.C., and Cook, K.R. (2012). The generation of chromosomal deletions to provide extensive coverage and subdivision of the Drosophila melanogaster genome. Genome Biol. *13*, R21.

Cull-Candy, S.G., Miledi, R., Trautmann, A., and Uchitel, O.D. (1980). On the release of transmitter at normal, myasthenia gravis and myasthenic syndrome affected human end-plates. J. Physiol. (Lond.) *299*, 621–638.

Davis, G.W. (2013). Homeostatic signaling and the stabilization of neural function. Neuron *80*, 718–728.

Davis, G.W., and Goodman, C.S. (1998). Synapse-specific control of synaptic efficacy at the terminals of a single neuron. Nature *392*, 82–86.

Davis, G.W., and Müller, M. (2015). Homeostatic control of presynaptic neurotransmitter release. Annu. Rev. Physiol. *77*, 251–270.

Davis, G.W., and Murphey, R.K. (1994). Retrograde signaling and the development of transmitter release properties in the invertebrate nervous system. J. Neurobiol. *25*, 740–756.

844 Deák, F., Xu, Y., Chang, W.-P., Dulubova, I., Khvotchev, M., Liu, X., Südhof,
845 T.C., and Rizo, J. (2009). Munc18-1 binding to the neuronal SNARE
846 complex controls synaptic vesicle priming. J. Cell Biol. *184*, 751–764.
847 Dietzl, G., Chen, D., Schnorrer, F., Su, K.-C., Barinova, Y., Fellner, M., Gasser,
848 B., Kinsey, K., Oppel, S., Scheiblauer, S., et al. (2007). A genome-wide
849 transgenic RNAi library for conditional gene inactivation in Drosophila.
850 Nature *448*, 151–156.
851 Dulubova, I., Khvotchev, M., Liu, S., Huryeva, I., Sudhof, T.C., and Rizo, J.
852 (2007). Munc18-1 binds directly to the neuronal SNARE complex.
853 Proceedings of the National Academy of Sciences *104*, 2697–2702.
854 Fisher, R.J., Pevsner, J., and Burgoyne, R.D. (2001). Control of fusion pore
855 dynamics during exocytosis by Munc18. Science *291*, 875–878.
856 Frank, C.A., Kennedy, M.J., Goold, C.P., Marek, K.W., and Davis, G.W. (2006).
857 Mechanisms underlying the rapid induction and sustained expression of
858 synaptic homeostasis. Neuron *52*, 663–677.
859 Frank, C.A., Pielage, J., and Davis, G.W. (2009). A presynaptic homeostatic
860 signaling system composed of the Eph receptor, ephexin, Cdc42, and
861 CaV2.1 calcium channels. Neuron *61*, 556–569.
862 Genc, O., Kochubey, O., Toonen, R.F., Verhage, M., and Schneggenburger, R.
863 (2014). Munc18-1 is a dynamically regulated PKC target during short-term
864 enhancement of transmitter release. Elife *3*, e01715.
865 Goold, C.P., and Davis, G.W. (2007). The BMP ligand Gbb gates the expression
866 of synaptic homeostasis independent of synaptic growth control. Neuron *56*,
867 109–123.
868 Graham, M.E., Barclay, J.W., and Burgoyne, R.D. (2004). Syntaxin/Munc18
869 interactions in the late events during vesicle fusion and release in
870 exocytosis. J. Biol. Chem. *279*, 32751–32760.
871 Gulyás-Kovács, A., de Wit, H., Milosevic, I., Kochubey, O., Toonen, R., Klingauf,
872 J., Verhage, M., and Sørensen, J.B. (2007). Munc18-1: sequential
873 interactions with the fusion machinery stimulate vesicle docking and
874 priming. J. Neurosci. *27*, 8676–8686.

875 Halachmi, N., Feldman, M., Kimchie, Z., and Lev, Z. (1995). Rop and Ras2,
876 members of the Sec1 and Ras families, are localized in the outer
877 membranes of labyrinthine channels and vesicles of Drosophila nephrocyte,
878 the Garland cell. Eur. J. Cell Biol. *67*, 275–283.
879 Harris, N., Braiser, D.J., Dickman, D.K., Fetter, R.D., Tong, A., and Davis, G.W.
880 (2015). The Innate Immune Receptor PGRP-LC Controls Presynaptic
881 Homeostatic Plasticity. Neuron *88*, 1157–1164.
882 Harrison, S.D., Broadie, K., van de Goor, J., and Rubin, G.M. (1994). Mutations
883 in the Drosophila Rop gene suggest a function in general secretion and
884 synaptic transmission. Neuron *13*, 555–566.
885 Hata, Y., and Südhof, T.C. (1995). A novel ubiquitous form of Munc-18 interacts
886 with multiple syntaxins. Use of the yeast two-hybrid system to study
887 interactions between proteins involved in membrane traffic. J. Biol. Chem.
888 *270*, 13022–13028.
889 Hata, Y., Slaughter, C.A., and Südhof, T.C. (1993). Synaptic vesicle fusion
890 complex contains unc-18 homologue boundto syntaxin. Nature *366*, 347–
891 351.
892 Hauswirth, A.G., Ford, K.J., Wang, T., Fetter, R.D., Tong, A., and Davis, G.W.
893 (2018). A postsynaptic PI3K-cII dependent signaling controller for
894 presynaptic homeostatic plasticity. Elife *7*.
895 He, E., Wierda, K., van Westen, R., Broeke, J.H., Toonen, R.F., Cornelisse, L.N.,
896 and Verhage, M. (2017). Munc13-1 and Munc18-1 together prevent NSF-
897 dependent de-priming of synaptic vesicles. Nat Commun *8*, 15915.
898 Henry, F.E., McCartney, A.J., Neely, R., Perez, A.S., Carruthers, C.J.L.,
899 Stuenkel, E.L., Inoki, K., and Sutton, M.A. (2012). Retrograde changes in
900 presynaptic function driven by dendritic mTORC1. J. Neurosci. *32*, 17128–
901 17142.
902 Jakawich, S.K., Nasser, H.B., Strong, M.J., McCartney, A.J., Perez, A.S.,
903 Rakesh, N., Carruthers, C.J.L., and Sutton, M.A. (2010). Local presynaptic
904 activity gates homeostatic changes in presynaptic function driven by
905 dendritic BDNF synthesis. Neuron *68*, 1143–1158.

Kaeser, P.S., and Regehr, W.G. (2014). Molecular Mechanisms for Synchronous, Asynchronous, and Spontaneous Neurotransmitter Release. Annual Review of Physiology *76*, 333–363.

Kim, S.H., and Ryan, T.A. (2010). CDK5 serves as a major control point in neurotransmitter release. Neuron *67*, 797–809.

Koushika, S.P., Richmond, J.E., Hadwiger, G., Weimer, R.M., Jorgensen, E.M., and Nonet, M.L. (2001). A post-docking role for active zone protein Rim. Nat. Neurosci. *4*, 997–1005.

Lee, J.S., Ho, W.-K., Neher, E., and Lee, S.-H. (2013). Superpriming of synaptic vesicles after their recruitment to the readily releasable pool. Proc. Natl. Acad. Sci. U.S.A. *110*, 15079–15084.

Lin, D.M., and Goodman, C.S. (1994). Ectopic and increased expression of Fasciclin II alters motoneuron growth cone guidance. Neuron *13*, 507–523.

Liu, G., and Tsien, R.W. (1995). Properties of synaptic transmission at single hippocampal synaptic boutons. Nature *375*, 404–408.

Liu, K.S.Y., Siebert, M., Mertel, S., Knoche, E., Wegener, S., Wichmann, C., Matkovic, T., Muhammad, K., Depner, H., Mettke, C., et al. (2011). RIM-binding protein, a central part of the active zone, is essential for neurotransmitter release. Science *334*, 1565–1569.

Misura, K.M., Scheller, R.H., and Weis, W.I. (2000). Three-dimensional structure of the neuronal-Sec1-syntaxin 1a complex. Nature *404*, 355–362.

Müller, M., Goutman, J.D., Kochubey, O., Schneggenburger, R. (2010). Interaction between facilitation and depression at a large CNS synapse reveals mechanisms of short-term plasticity. J Neurosci. *30(6)*, 2007–2016.

Müller, M., and Davis, G.W. (2012). Transsynaptic control of presynaptic Ca^{2+} influx achieves homeostatic potentiation of neurotransmitter release. Curr. Biol. *22*, 1102–1108.

Müller, M., Liu, K.S.Y., Sigrist, S.J., and Davis, G.W. (2012). RIM controls homeostatic plasticity through modulation of the readily-releasable vesicle pool. J. Neurosci. *32*, 16574–16585.

936 Müller, M., Genç, Ö., and Davis, G.W. (2015). RIM-binding protein links synaptic
937 homeostasis to the stabilization and replenishment of high release
938 probability vesicles. Neuron *85*, 1056–1069.
939 Orr, B.O., Fetter, R.D., and Davis, G.W. (2017). Retrograde semaphorin-plexin
940 signalling drives homeostatic synaptic plasticity. Nature *550*, 109–113.
941 Park, S., Bin, N.-R., Yu, B., Wong, R., Sitarska, E., Sugita, K., Ma, K., Xu, J.,
942 Tien, C.-W., Algouneh, A., et al. (2017). UNC-18 and Tomosyn
943 Antagonistically Control Synaptic Vesicle Priming Downstream of UNC-13 in
944 Caenorhabditis elegans. J. Neurosci. *37*, 8797–8815.
945 Patzke, C., Han, Y., Covy, J., Yi, F., Maxeiner, S., Wernig, M., and Südhof, T.C.
946 (2015). Analysis of conditional heterozygous STXBP1 mutations in human
947 neurons. J. Clin. Invest. *125*, 3560–3571.
948 Pevsner, J., Hsu, S.C., and Scheller, R.H. (1994). n-Sec1: a neural-specific
949 syntaxin binding protein. Proc. Natl. Acad. Sci. U.S.A. *91*, 1445–1449.
950 Plomp, J.J., van Kempen, G.T., and Molenaar, P.C. (1992). Adaptation of quantal
951 content to decreased postsynaptic sensitivity at single endplates in alpha-
952 bungarotoxin-treated rats. J. Physiol. (Lond.) *458*, 487–499.
953 Pouille, F., and Scanziani, M. (2004). Routing of spike series by dynamic circuits
954 in the hippocampus. Nature *429*, 717–723.
955 Riento, K., Kauppi, M., Keranen, S., and Olkkonen, V.M. (2000). Munc18-2, a
956 functional partner of syntaxin 3, controls apical membrane trafficking in
957 epithelial cells. J. Biol. Chem. *275*, 13476–13483.
958 Schlüter, O.M., Basu, J., Südhof, T.C., and Rosenmund, C. (2006). Rab3
959 superprimes synaptic vesicles for release: implications for short-term
960 synaptic plasticity. J. Neurosci. *26*, 1239–1246.
961 Schneggenburger, R., Meyer, A.C., and Neher, E. (1999). Released fraction and
962 total size of a pool of immediately available transmitter quanta at a calyx
963 synapse. Neuron *23*, 399–409.
964 Schulze, K.L., Broadie, K., Perin, M.S., and Bellen, H.J. (1995). Genetic and
965 electrophysiological studies of Drosophila syntaxin-1A demonstrate its role
966 in nonneuronal secretion and neurotransmission. Cell *80*, 311–320.

967 Smyth, A.M., Yang, L., Martin, K.J., Hamilton, C., Lu, W., Cousin, M.A., Rickman,
968 C., and Duncan, R.R. (2013). Munc18-1 Protein Molecules Move between
969 Membrane Molecular Depots Distinct from Vesicle Docking Sites. Journal of
970 Biological Chemistry *288*, 5102–5113.
971 Sons, M.S., Verhage, M., and Plomp, J.J. (2003). Role of Munc18-1 in synaptic
972 plasticity at the myasthenic neuromuscular junction. Ann. N. Y. Acad. Sci.
973 *998*, 404–406.
974 Südhof, T.C. (2012a). Calcium Control of Neurotransmitter Release. Cold Spring
975 Harbor Perspectives in Biology *4*, a011353–a011353.
976 Südhof, T.C. (2012b). The presynaptic active zone. Neuron *75*, 11–25.
977 Taschenberger, H., Woehler, A., and Neher, E. (2016). Superpriming of synaptic
978 vesicles as a common basis for intersynapse variability and modulation of
979 synaptic strength. Proc. Natl. Acad. Sci. U.S.A. *113*, E4548-4557.
980 Thiagarajan, T.C., Lindskog, M., and Tsien, R.W. (2005). Adaptation to synaptic
981 inactivity in hippocampal neurons. Neuron *47*, 725–737.
982 Toonen, R.F.G., and Verhage, M. (2003). Vesicle trafficking: pleasure and pain
983 from SM genes. Trends Cell Biol. *13*, 177–186.
984 Toonen, R.F.G., and Verhage, M. (2007). Munc18-1 in secretion: lonely Munc
985 joins SNARE team and takes control. Trends Neurosci. *30*, 564–572.
986 Toonen, R.F.G., Wierda, K., Sons, M.S., de Wit, H., Cornelisse, L.N., Brussaard,
987 A., Plomp, J.J., and Verhage, M. (2006). Munc18-1 expression levels
988 control synapse recovery by regulating readily releasable pool size. Proc.
989 Natl. Acad. Sci. U.S.A. *103*, 18332–18337.
990 Von der Malsburg C, Bienenstock E (1986). Statistical coding and short-term
991 synaptic plasticity: A scheme for knowledge representation in the brain.
992 Disordered Systems and Biological Organization, eds Bienenstock E,
993 Fogelman-Soulié F, Weisbuch G (Springer, Berlin), pp. 247–272.
994 Verhage, M., Maia, A.S., Plomp, J.J., Brussaard, A.B., Heeroma, J.H., Vermeer,
995 H., Toonen, R.F., Hammer, R.E., van den Berg, T.K., Missler, M., et al.
996 (2000). Synaptic assembly of the brain in the absence of neurotransmitter
997 secretion. Science *287*, 864–869.

998 Voets, T., Toonen, R.F., Brian, E.C., de Wit, H., Moser, T., Rettig, J., Südhof,
999 T.C., Neher, E., and Verhage, M. (2001). Munc18-1 promotes large dense-
1000 core vesicle docking. Neuron *31*, 581–591.
1001 Wang, X., and Rich, M.M. (2018). Homeostatic synaptic plasticity at the
1002 neuromuscular junction in myasthenia gravis. Ann. N. Y. Acad. Sci. *1412*,
1003 170–177.
1004 Wang, H.-L., Zhang, Z., Hintze, M., and Chen, L. (2011). Decrease in calcium
1005 concentration triggers neuronal retinoic acid synthesis during homeostatic
1006 synaptic plasticity. J. Neurosci. *31*, 17764–17771.
1007 Wang, T., Jones, R.T., Whippen, J.M., and Davis, G.W. (2016). α2δ-3 Is
1008 Required for Rapid Transsynaptic Homeostatic Signaling. Cell Reports *16*,
1009 2875–2888.
1010 Wang, Y., Sugita, S., and Sudhof, T.C. (2000). The RIM/NIM family of neuronal
1011 C2 domain proteins. Interactions with Rab3 and a new class of Src
1012 homology 3 domain proteins. J. Biol. Chem. *275*, 20033–20044.
1013 Weimer, R.M., Richmond, J.E., Davis, W.S., Hadwiger, G., Nonet, M.L., and
1014 Jorgensen, E.M. (2003). Defects in synaptic vesicle docking in unc-18
1015 mutants. Nat. Neurosci. *6*, 1023–1030.
1016 Weyhersmüller, A., Hallermann, S., Wagner, N., and Eilers, J. (2011). Rapid
1017 active zone remodeling during synaptic plasticity. J. Neurosci. *31*, 6041–
1018 6052.
1019 Wu, M.N., Littleton, J.T., Bhat, M.A., Prokop, A., and Bellen, H.J. (1998). ROP,
1020 the Drosophila Sec1 homolog, interacts with syntaxin and regulates
1021 neurotransmitter release in a dosage-dependent manner. EMBO J. *17*, 127–
1022 139.
1023 Younger, M.A., Müller, M., Tong, A., Pym, E.C., and Davis, G.W. (2013). A
1024 presynaptic ENaC channel drives homeostatic plasticity. Neuron *79*, 1183–
1025 1196.
1026 Zhao, C., Dreosti, E., and Lagnado, L. (2011). Homeostatic synaptic plasticity
1027 through changes in presynaptic calcium influx. J. Neurosci. *31*, 7492–7496.

Zucker, R.S., and Regehr, W.G. (2002). Short-term synaptic plasticity. Annu. Rev. Physiol. *64*, 355–405.

Figure Legends

Figure 1 Preservation of Release Dynamics During Presynaptic Homeostatic Plasticity. (A) Example traces at the indicated external calcium concentration in the presence or absence of PhTx and PdBu. **(B)** Paired-pulse ratio (EPSC4/EPSC1) versus initial EPSC amplitude (EPSC1) at two external calcium concentrations as indicated. **(C)** Data from (B) re-plotted (gray) with the addition of data recorded in the presence of PhTx (light and dark red) for indicated external calcium concentrations. **(D)** Data from (B) re-plotted (gray) with the addition of data recorded in the presence of PdBu (light and dark blue) for indicated external calcium concentrations. **(E)** Data for mEPSP, EPSC and quantal content for control (ctrl), control in the presence of PdBu (PdBu), control in the presence of PhTx (PhTx) and control synapses incubated in PhTx followed by PdBU (PhTx+PdBu). At right, percent change is calculated as quantal content recorded in the presence of PdBu versus control in the absence of PdBu. **(F)** EPSC amplitude in the presence (red) and absence (black) of PdBu at the indicated extracellular calcium concentrations. **(G)** Schematic highlighting the homeostatic doubling of the pool of docked primed vesicles during presynaptic homeostatic plasticity (PHP) in the presence of PhTx. The ratio of primed (light red) to super-primed (dark red) vesicles is held constant, thereby preserving presynaptic release dynamics. ns, not significant; *p<0.05, **p<0.01, ***p<0.001; Data represent mean ± SEM. Student's t-test, two tailed.

Figure 2. Identification of Rop as a SNARE-Associated Molecule Involved in the Rapid Induction of Presynaptic Homeostasis. (A) Schematic of the *Drosophila Rop* gene locus (top) and protein (bottom). Coding exon is shown in dark purple and non-coding DNA is in gray. Protein is shown in light purple. Point mutations in *Rop* mutant alleles (Rop^{G27} and Rop^{G11}) are indicated by red stars. Deficiency Df(3L)BSC735 uncovers the *Rop* gene locus as indicated. syntaxin-binding domains (SBD) of the Rop protein are shown (pink). **(B)** Average data for mEPSP amplitude in the absence (baseline) and presence (PhTx) of PhTx for WT and heterozygous deficiency chromosome *Df(3L)BSC735* (Df^{Rop}/+). PhTx application reduces amplitudes in all genotypes (p<0.01). Data represent mean ± SEM. **(C)** Average data for EPSP amplitude as in (B); sample sizes for data in (B-D) are shown on bar graph; ns, not significant; *p<0.05; Student's t-test. **(D)** Average mEPSP amplitude and quantal content are normalized to values in the absence of PhTx for each genotype. ***p<0.001. **(E)** Sample traces showing EPSP and mEPSP amplitudes ± PhTx for indicated genotypes. **(F-H)** Average mEPSP (F) EPSP (G) and Quantal Content (H) for indicated genotypes; ns, not significant; ****p<0.0001; **p<0.01. **(I)** Average percent change in mEPSP amplitude and quantal content in PhTx compared to baseline for indicated genotypes; **p<0.01. Data are mean ± SEM for all figures. Student's t-test, two tailed.

Figure 3. Rop is Required Neuronally During Presynaptic Homeostasis. **(A)** Sample traces showing EPSP and mEPSP amplitudes ± PhTx for indicated genotypes. **(B)** Average data for mEPSP when *UAS-Rop-RNAi* is expressed pan-neuronally (*c155-GAL4*) ± Phtx as indicated. PhTx reduces amplitudes in all genotypes; p<0.01. **(C)** Average data for EPSP as in B; ns, not significant; **p<0.01. **(D)** Average data for Quantal Content as in B; **p<0.01. **(E)** Average percent change in mEPSP amplitude and quantal content in PhTx compared to baseline for indicated genotypes; ***p<0.001. **(F)** Sample traces showing mEPSPs for indicated genotypes (left) and average mEPSP frequencies (Hz) (right). Student's t-test, two tailed.

Figure 4. Suppression of Presynaptic Homeostasis is maintained with increased $[Ca^{2+}]_e$ in *Rop* mutants. (A) Sample EPSC traces in the absence (baseline) and presence (PhTx) of PhTx for WT and heterozygous Rop^{G27} mutant at 1.5 mM extracellular calcium $[Ca^{2+}]_e$. **(B)** Average data for mEPSP amplitude ± PhTx for indicated genotypes. PhTx application reduces amplitude in all genotypes (p<0.01). Data represent mean ± SEM. **(C)** Average data for EPSC amplitude as in (B); ns, not significant; **p<0.01, *p<0.05; Student's t test, two tailed. Sample sizes indicated on bar graph. **(D-E)** Average mEPSP (D) EPSC (E) ± PhTx for each genotype at 3.0 mM extracellular calcium $[Ca^{2+}]_e$; ns, not significant; **p<0.01; Data represent mean ± SEM. Student's t-test, two tailed. **(F)** Relationship between mean quantal content and $[Ca^{2+}]_e$ (left axis) and relationship between quantal content normalized to values in the absence of PhTx and $[Ca^{2+}]_e$ (right axis) for WT and Rop^{G27} heterozygous mutants.

Figure 5. Decreased Release Probability in *Rop* Mutants. (A) Sample EPSC traces (top) and cumulative EPSC amplitudes (bottom) ± PhTx for indicated genotypes. Experiment used 60 Hz stimulation (30 stimuli) in 1.5 mM $[Ca^{2+}]_e$. Red line is fit to cumulative EPSC data and back extrapolated to time zero. **(B)** Average cumulative EPSC amplitudes ± PhTx for indicated genotypes; ns, not significant. Student's t-test, two tailed. **(C)** Average P_{train} ± PhTx for indicated genotypes. P_{train} = 1st EPSC / cumEPSC; ns, not significant; ***p<0.001. **(D)** Average EPSC amplitudes normalized to the first pulse are plotted against stimulus number for indicated genotypes.

Figure 6. *Rop* Interacts with *rim* during Synaptic Homeostasis. (A) Average data for mEPSP amplitude ± PhTx for WT, heterozygous Rop^{G27}/+ mutant heterozygous rim^{103}/+ mutant, and transheterozygous Rop^{G27}/rim^{103} mutant at 0.3 mM $[Ca^{2+}]_e$. PhTx application reduces amplitude in all genotypes (p<0.01). Data represent mean ± SEM. Student's t test. **(B)** Average data for EPSP amplitude ± PhTx for indicated genotypes; statistics as in (A); *p<0.05; ***p<0.001; ****p<0.0001, Student's t-test, two tailed. **(C)** Average data for Quantal Content ± PhTx for indicated genotypes as in (A); ns, not significant; **p<0.01; ****p<0.0001; Student's t-test, two tailed. **(D)** Average data for mEPSP and quantal content normalized to values in the absence of PhTx for indicated

genotypes. Statistical comparisons are made within each genotype to baseline in the absence of PhTx. Student's t-test, two tailed**. (E)** Each point represents average data from an individual NMJ recording. For WT, recordings in the absence of PhTx are dark gray, those with PhTx are light gray. For Rop^{G27}/+, recordings in the absence of PhTx are dark purple, those with PhTx are light purple. For rim^{103}/+, recordings in the absence of PhTx are dark blue, those with PhTx are light blue. For Rop^{G27}/rim^{103}, recordings in the absence of PhTx are dark red, those with PhTx are light red. The black line in the WT graph is a curve fit to this control data. The same wild type curve-fit is overlaid on all other genotypes for purposes of comparison. Dotted black lines encompass 95% of wild type data points. These same lines from wild type are superimposed on the graphs for indicated genotypes. **(F-H)** Average percent change in mEPSP amplitude and quantal content in PhTx compared to baseline for trans heterozygous combinations: Rop^{G27}/rbp^{STOP1} (F), rim^{103}/+; $dunc13^{P84200}$/+ (G), rim^{103}/rbp^{STOP1} (H); ns, not significant; *p<0.05; Student's t-test, two tailed.

Figure 7. Enhanced action of PdBu at synapses depleted of both Rop and RIM. (A) Paired-pulse ratio is plotted against initial EPSC amplitude for the indicated genotypes and conditions (in the absence and presence of PdBu). **(B)** Representative traces for the indicated genotypes in the absence (baseline) and presence of PdBu (PdBu, red). **(C)** The effect of PdBu application is plotted for wild type controls, the Rop^{G27}/rim^{103} double heterozygous condition and each heterozygous mutation alone. Each genotype is expressed as a percent change in the presence compared to absence of PdBu. Calculations are made on the first EPSC of the stimulus train (EPSC1). The average percent change is statistically significant only in the double heterozygous condition (p<0.01; ANOVA, One Way with Tukey Multiple Comparisons). **(D)** Data as in (C) plotting the ratio of EPSC4/EPSC1 as a percent change in the presence compared to absence of PdBu. The average percent change is statistically significant only in the double heterozygous condition (p<0.01; ANOVA, One Way with Tukey Multiple Comparisons).

Figure 8. *Syx* rescues PHP during Synaptic Homeostasis. (A) Sample traces showing EPSP and mEPSP amplitudes in the absence (baseline) and presence (PhTx) of PhTx for *syx1A* heterozygous null allele ($syx1A^{\Delta 229}$/+) and heterozygous $syx1A^{\Delta 229}$ placed in trans with Rop^{G27} mutant ($Rop^{G27}/syx1A^{\Delta 229}$). **(B)** Average data for mEPSP amplitude ± PhTx for indicated genotypes. PhTx application reduces amplitude in all genotypes (p<0.01). Data represent mean ± SEM. Student's t test. **(C-E)** Average data for EPSP amplitude (C) Quantal Content (D) and mEPSP and quantal content normalized to values in the absence of PhTx (E) for indicated genotypes. Statistical comparisons are made to wild type for each genotype in (E). ** p<0.01; **** p<0.0001, Student's t-test, two tailed. **(F)** Average mEPSP frequencies (Hz) (left) and sample traces showing mEPSPs for indicated genotypes (right). Student's t test, two tailed.

Figure 9. *Rop^{G11}* abolishes biochemical interaction between Rop and syx1A and rescues homeostasis defect in Rop. (A) Schematic of the *Drosophila* Rop protein. Point mutation *Rop^{G11}* is indicated by red star at syntaxin-binding domain (SBD) of the Rop protein shown in pink. *Rop^{G11}* converts Aspartic Acid (D45) to Asparagine (N). This site is conserved in mammalian *Rop (munc18-1)*.
(B) Coomassie stains of *in vitro* binding assays. (left) MBP-Rop (110kDa) coprecipitated with bead-bound GST fusions of syx1A (GST-syx1A$^{\Delta C}$) (60kDa). MBP-Rop does not bind to GST-syx1A$^{\Delta C}$ in the presence of single point mutation at the N-terminal of Rop (MBP-Rop^{G11}). (right) Free MBP-Rop in the absence of GST-syx1A. **(C)** Binding Curves quantify dissociation constant (K_d) for MBP-Rop and MBP-Rop^{G11} binding to GST-syx1A$^{\Delta C}$; x-axis is concentration of MBP recombinant protein used (μM); y-axis is the fraction of protein bound; n = 2
(D) Sample traces showing EPSC amplitudes ± PhTx for *Rop^{G11}* heterozygous null allele (*Rop^{G11}*/+), heterozygous *Rop^{G11}* placed in trans with *Rop^{G27}* mutant (*Rop^{G27}/ Rop^{G11}*), and heterozygous *Rop^{G11}* placed in trans with *Df^{Rop} (Df^{Rop}/ Rop^{G11}).* **(E)** Average data for mEPSP amplitude ± PhTx for indicated genotypes. PhTx application reduces amplitude in all genotypes ($p<0.01$). Data represent mean ± SEM. Student's t test. two tailed. **(F)** Average data for EPSC amplitude as in (B); ns, not significant; Student's t test, two tailed.

Supplemental Figure Legends:

Figure 1 – figure supplement 1. PdBu-dependent potentiation converges to wild type steady state during a prolonged stimulus train. Average peak amplitudes of 60 Hz trains in the absence (black) and presence (red) of PdBu (n=6 for control, n=4 for PdBu, data are mean ± SEM). The average of the last three data points at the end of the stimulus trains are statistically similar ($p>0.1$; Student's t-test, two tails).

Supplemental Files, File title:

Supplementary File 1. Supplemental Table 1. Summary of raw data.

Figure 1

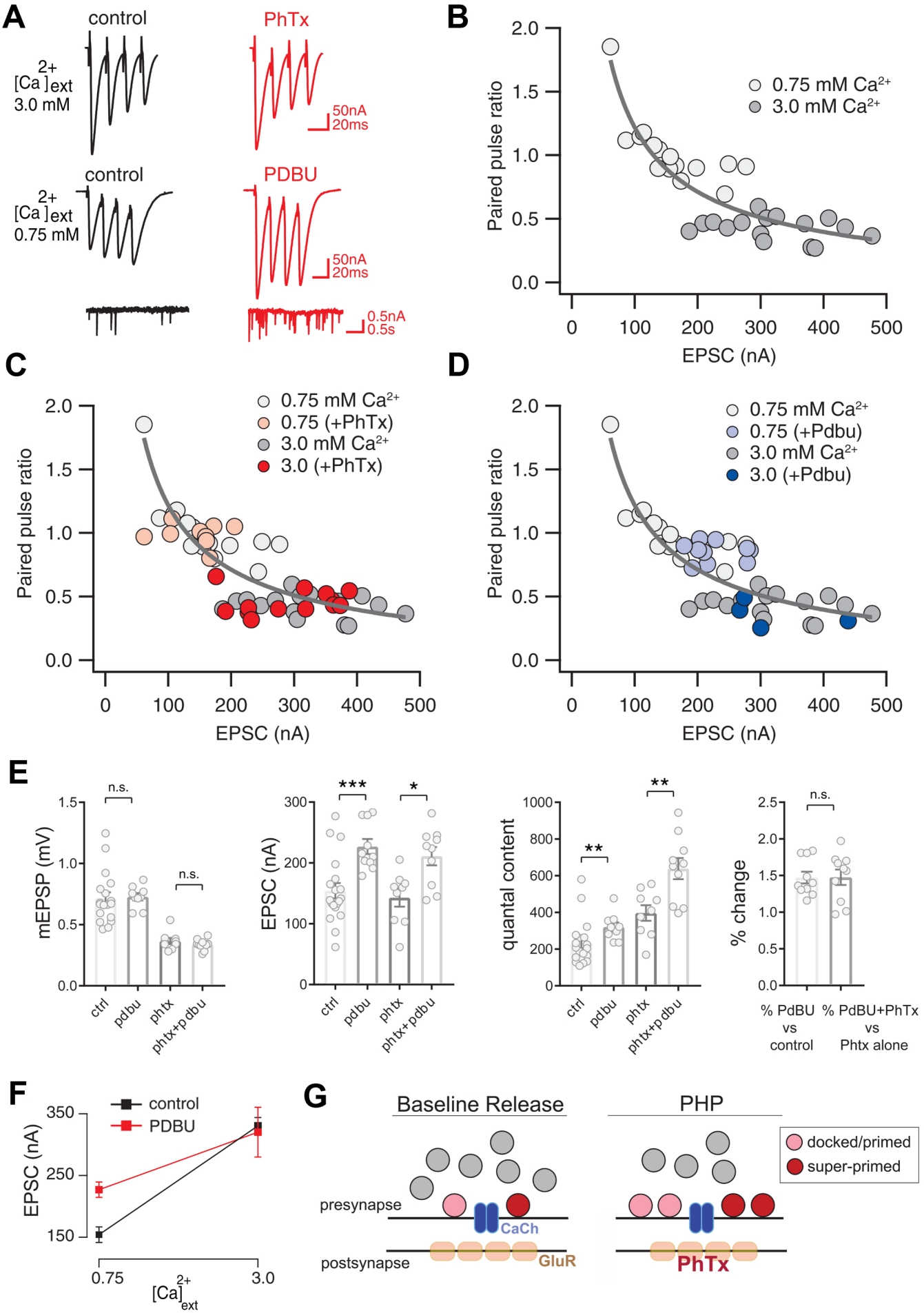
A
control
PhTx
2+
[Ca]ext
3.0 mM
50nA
20ms
control
PDBU
2+
[Ca]ext
0.75 mM
50nA
20ms
0.5nA
0.5s
B
Paired pulse ratio
EPSC (nA)
0.75 mM Ca2+
3.0 mM Ca2+
C
Paired pulse ratio
EPSC (nA)
0.75 mM Ca2+
0.75 (+PhTx)
3.0 mM Ca2+
3.0 (+PhTx)
D
Paired pulse ratio
EPSC (nA)
0.75 mM Ca2+
0.75 (+Pdbu)
3.0 mM Ca2+
3.0 (+Pdbu)
E
mEPSP (mV)
n.s.
n.s.
ctrl
pdbu
phtx
phtx+pdbu
EPSC (nA)
***
*
quantal content
**
**
% change
n.s.
% PdBU vs control
% PdBU+PhTx vs Phtx alone
F
EPSC (nA)
control
PDBU
0.75
3.0
[Ca]2+ext
G
Baseline Release
PHP
docked/primed
super-primed
presynapse
CaCh
postsynapse
GluR
PhTx

Figure 2

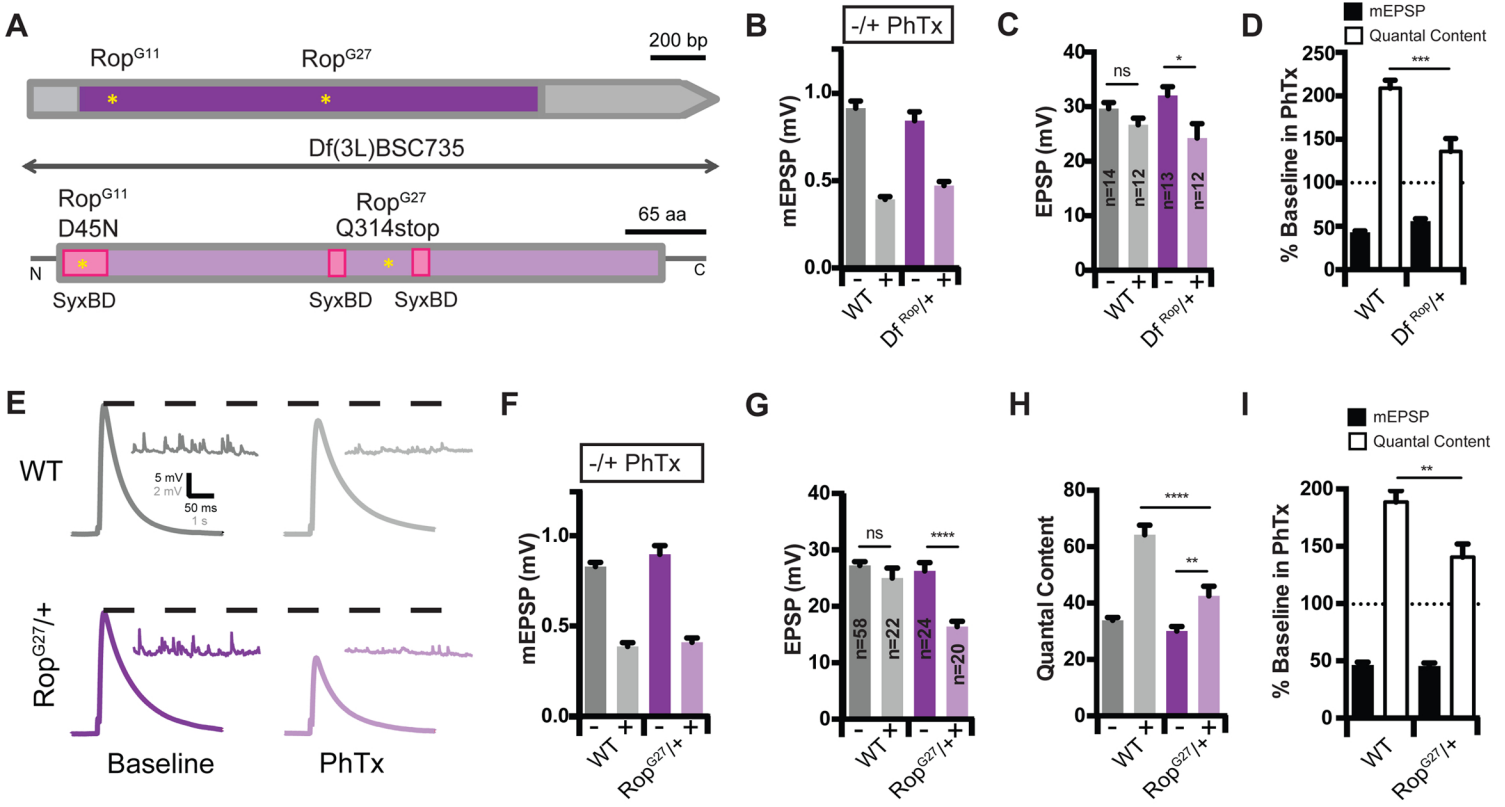
A
Rop^G11
Rop^G27
200 bp
Df(3L)BSC735
Rop^G11
D45N
Rop^G27
Q314stop
65 aa
N
C
SyxBD
SyxBD
SyxBD
B
-/+ PhTx
mEPSP (mV)
1.0
0.5
0.0
- + - +
WT
Df Rop/+
C
EPSP (mV)
40
30
20
10
0
ns
*
n=14
n=12
n=13
n=12
- + - +
WT
Df Rop/+
D
mEPSP
Quantal Content
% Baseline in PhTx
250
200
150
100
50
0
***
WT
Df Rop/+
E
WT
5 mV
2 mV
50 ms
1 s
Rop^G27/+
Baseline
PhTx
F
-/+ PhTx
mEPSP (mV)
1.0
0.5
0.0
- + - +
WT
Rop^G27/+
G
EPSP (mV)
40
30
20
10
0
ns
****
n=58
n=22
n=24
n=20
- + - +
WT
Rop^G27/+
H
Quantal Content
80
60
40
20
0
****
**
- + - +
WT
Rop^G27/+
I
mEPSP
Quantal Content
% Baseline in PhTx
200
150
100
50
0
**
WT
Rop^G27/+

Figure 3

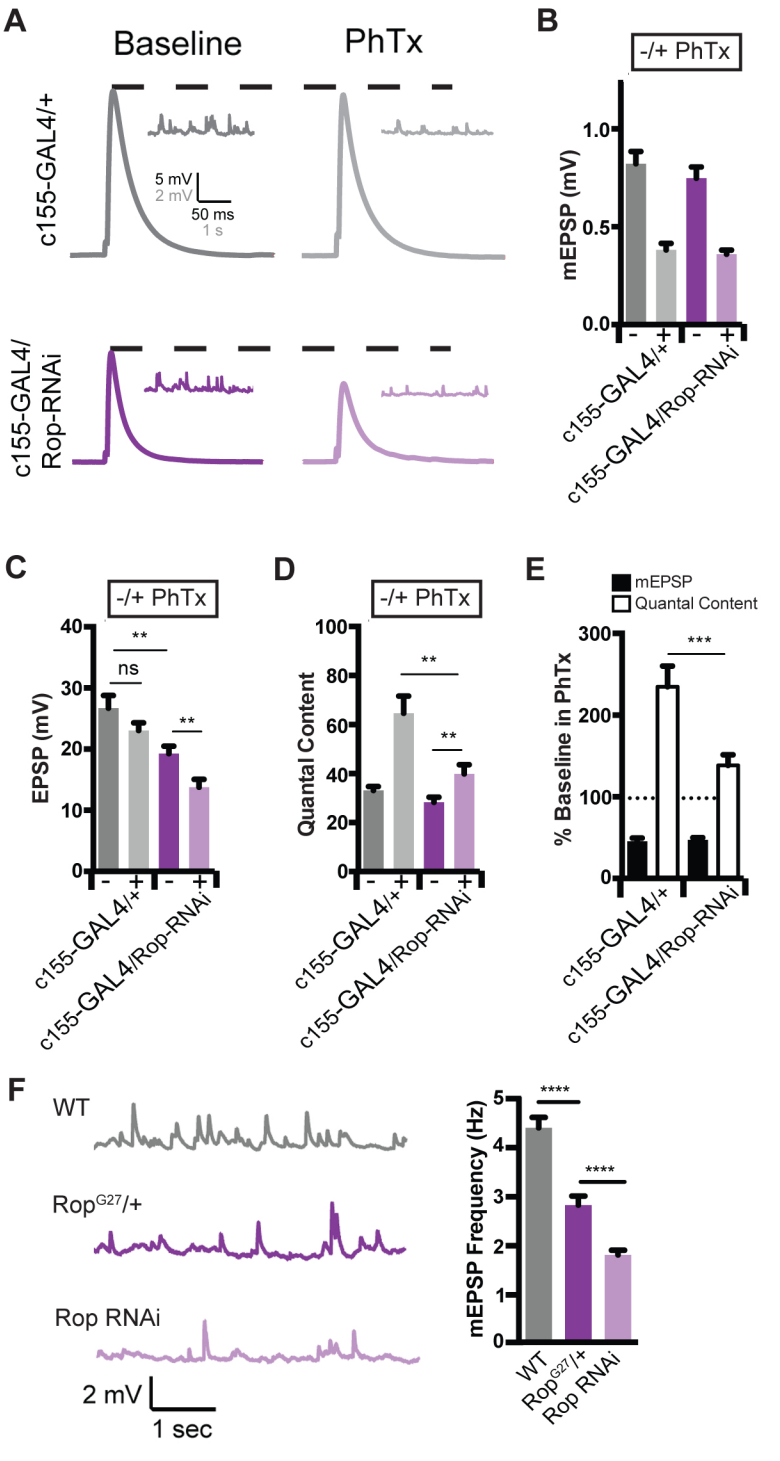
A
Baseline
PhTx
c155-GAL4/+
5 mV
2 mV
50 ms
1 s
c155-GAL4/
Rop-RNAi
B
-/+ PhTx
mEPSP (mV)
1.0
0.5
0.0
- + - +
c155-GAL4/+
c155-GAL4/Rop-RNAi
C
-/+ PhTx
EPSP (mV)
40
30
20
10
0
**
ns
**
- + - +
c155-GAL4/+
c155-GAL4/Rop-RNAi
D
-/+ PhTx
Quantal Content
100
80
60
40
20
0
**
**
- + - +
c155-GAL4/+
c155-GAL4/Rop-RNAi
E
mEPSP
Quantal Content
% Baseline in PhTx
300
200
100
0
***
c155-GAL4/+
c155-GAL4/Rop-RNAi
F
WT
Rop^G27/+
Rop RNAi
2 mV
1 sec
mEPSP Frequency (Hz)
5
4
3
2
1
0
****
****
WT
Rop^G27/+
Rop RNAi

Figure 4

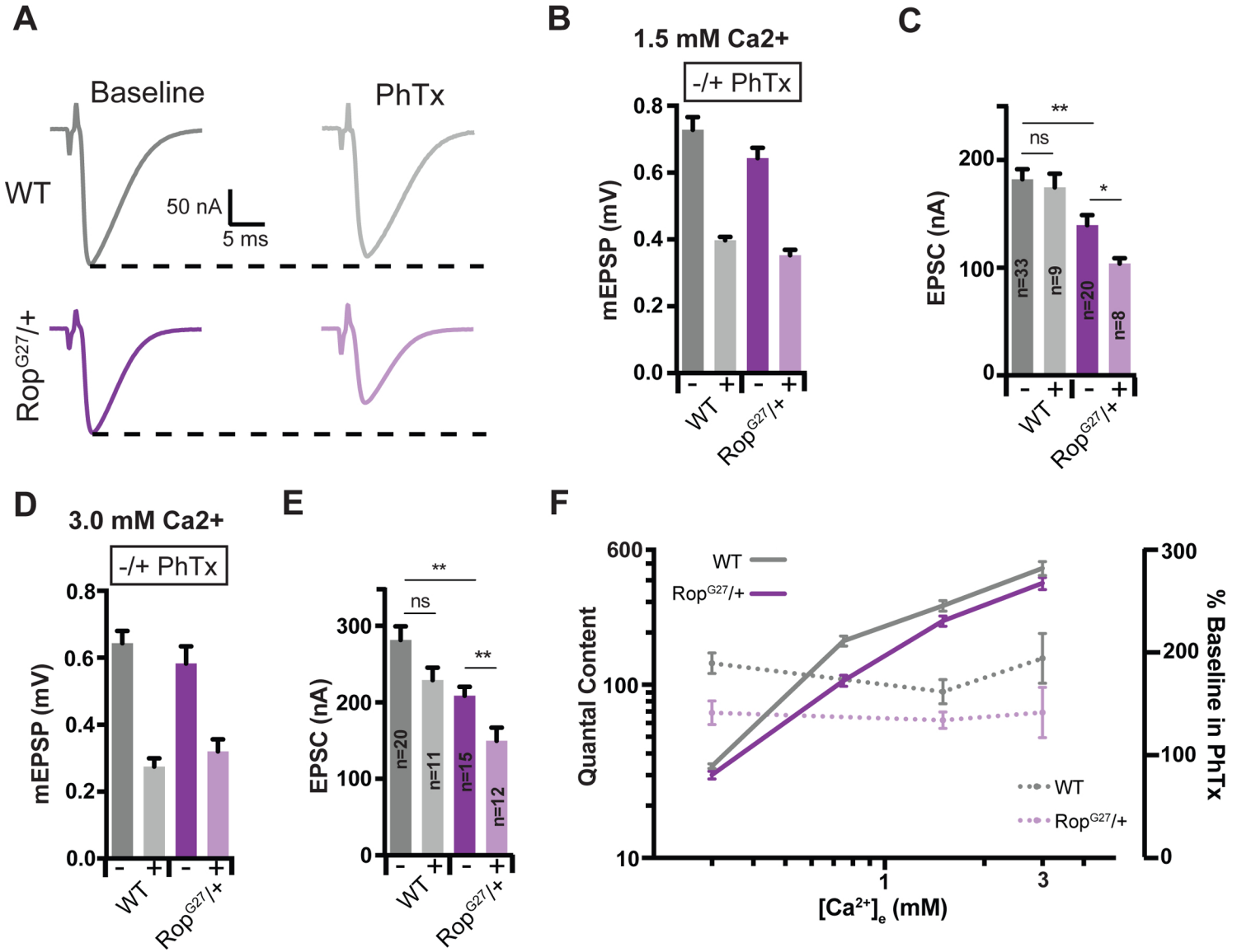
A
Baseline
PhTx
WT
50 nA
5 ms
RopG27/+
B
1.5 mM Ca2+
-/+ PhTx
mEPSP (mV)
0.8
0.6
0.4
0.2
0.0
- + - +
WT
RopG27/+
C
EPSC (nA)
200
100
0
**
ns
*
n=33
n=9
n=20
n=8
- + - +
WT
RopG27/+
D
3.0 mM Ca2+
-/+ PhTx
mEPSP (mV)
0.8
0.6
0.4
0.2
0.0
- + - +
WT
RopG27/+
E
EPSC (nA)
300
200
100
0
**
ns
**
n=20
n=11
n=15
n=12
- + - +
WT
RopG27/+
F
Quantal Content
600
100
10
WT
RopG27/+
1
3
[Ca2+]e (mM)
WT
RopG27/+
% Baseline in PhTx
300
200
100
0

Figure 5

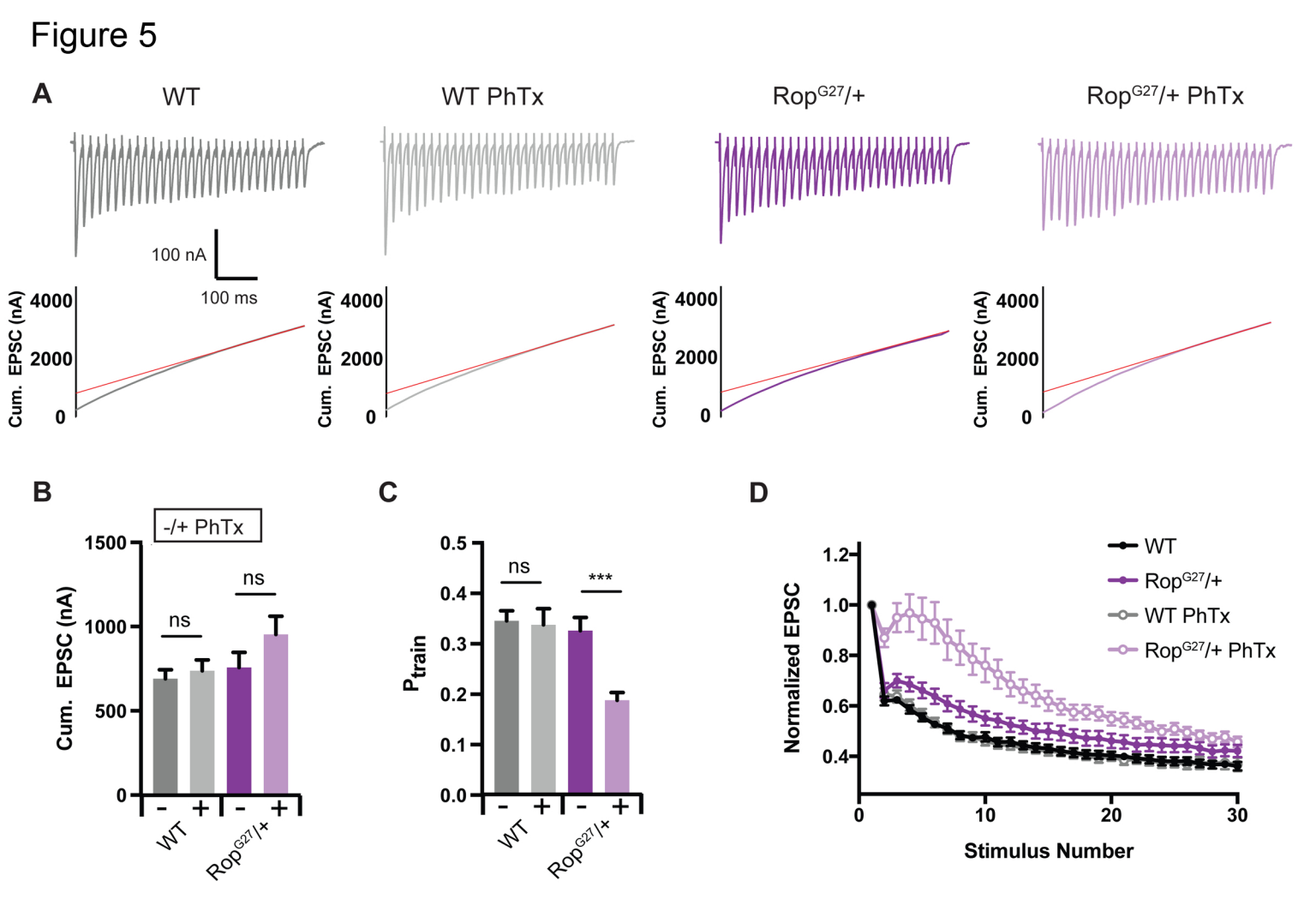
A
WT
WT PhTx
Rop^{G27}/+
Rop^{G27}/+ PhTx
100 nA
100 ms
Cum. EPSC (nA)
4000
2000
0
B
-/+ PhTx
Cum. EPSC (nA)
1500
1000
500
0
ns
ns
- + - +
WT
Rop^{G27}/+
C
P_{train}
0.5
0.4
0.3
0.2
0.1
0.0
ns
***
- + - +
WT
Rop^{G27}/+
D
Normalized EPSC
1.2
1.0
0.8
0.6
0.4
0
10
20
30
Stimulus Number
WT
Rop^{G27}/+
WT PhTx
Rop^{G27}/+ PhTx

Figure 6

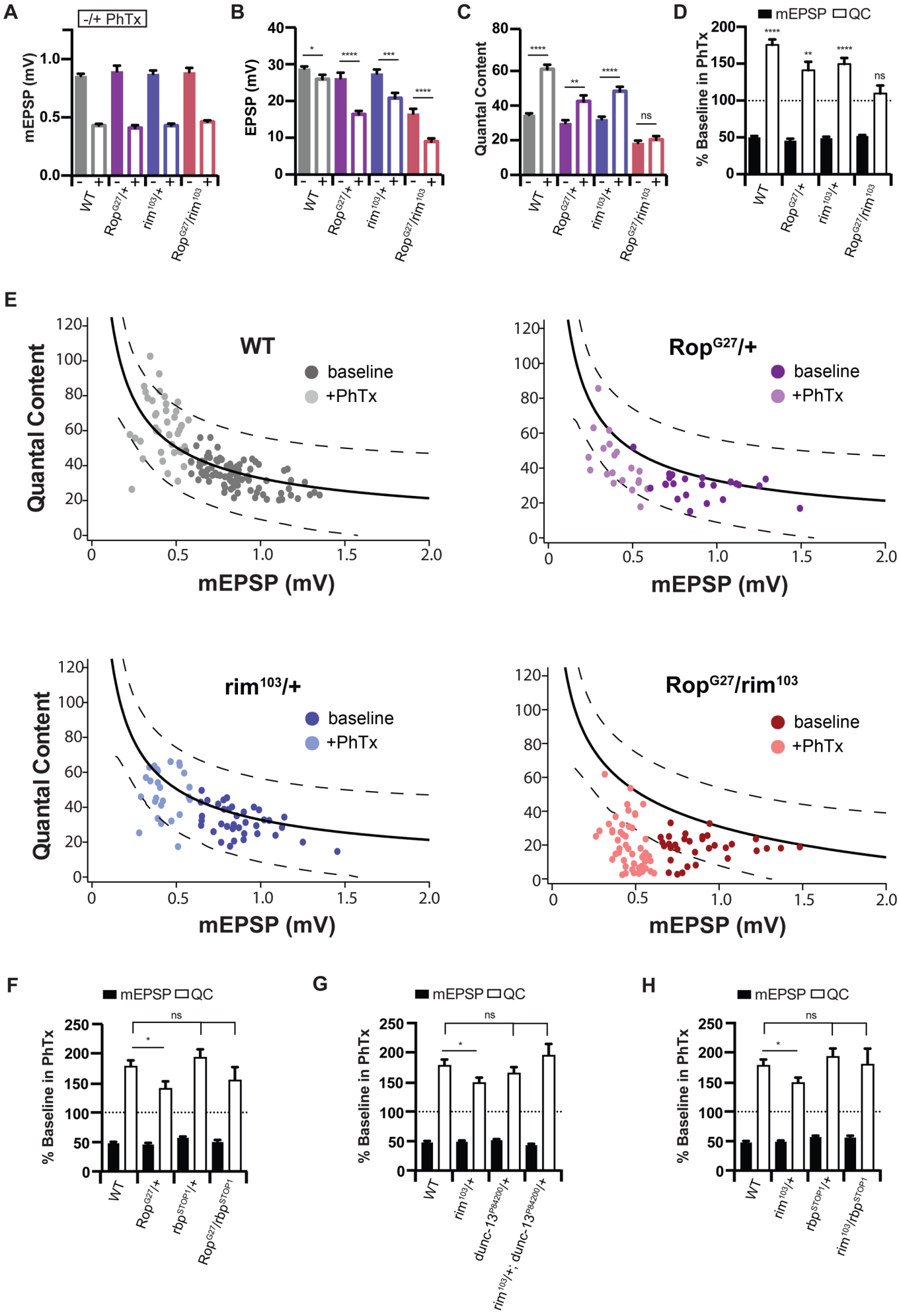
A
-/+ PhTx
mEPSP (mV)
WT
Rop^G27/+
rim^103/+
Rop^G27/rim^103
B
EPSP (mV)
C
Quantal Content
D
mEPSP QC
% Baseline in PhTx
E
WT
baseline
+PhTx
Rop^G27/+
rim^103/+
Rop^G27/rim^103
Quantal Content
mEPSP (mV)
F
rbp^STOP1/+
Rop^G27/rbp^STOP1
G
dunc-13^P84200/+
rim^103/+; dunc-13^P84200/+
H
rim^103/rbp^STOP1
ns

Figure 7

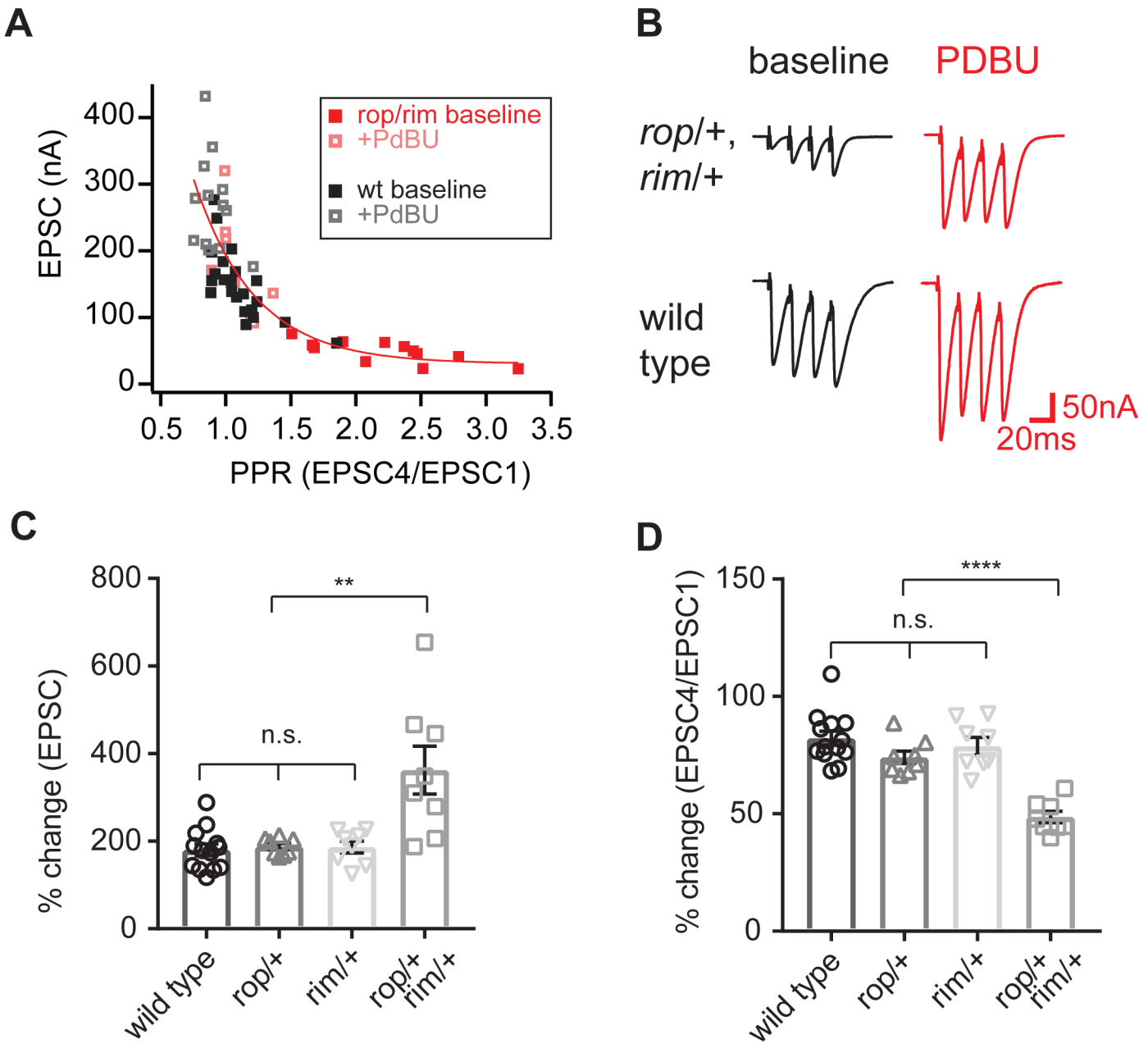
A
EPSC (nA)
400
300
200
100
0
0.5
1.0
1.5
2.0
2.5
3.0
3.5
PPR (EPSC4/EPSC1)
rop/rim baseline
+PdBU
wt baseline
+PdBU
B
baseline
PDBU
rop/+,
rim/+
wild
type
50nA
20ms
C
% change (EPSC)
800
600
400
200
0
**
n.s.
wild type
rop/+
rim/+
rop/+
rim/+
D
% change (EPSC4/EPSC1)
150
100
50
0
****
n.s.
wild type
rop/+
rim/+
rop/+
rim/+

Figure 8

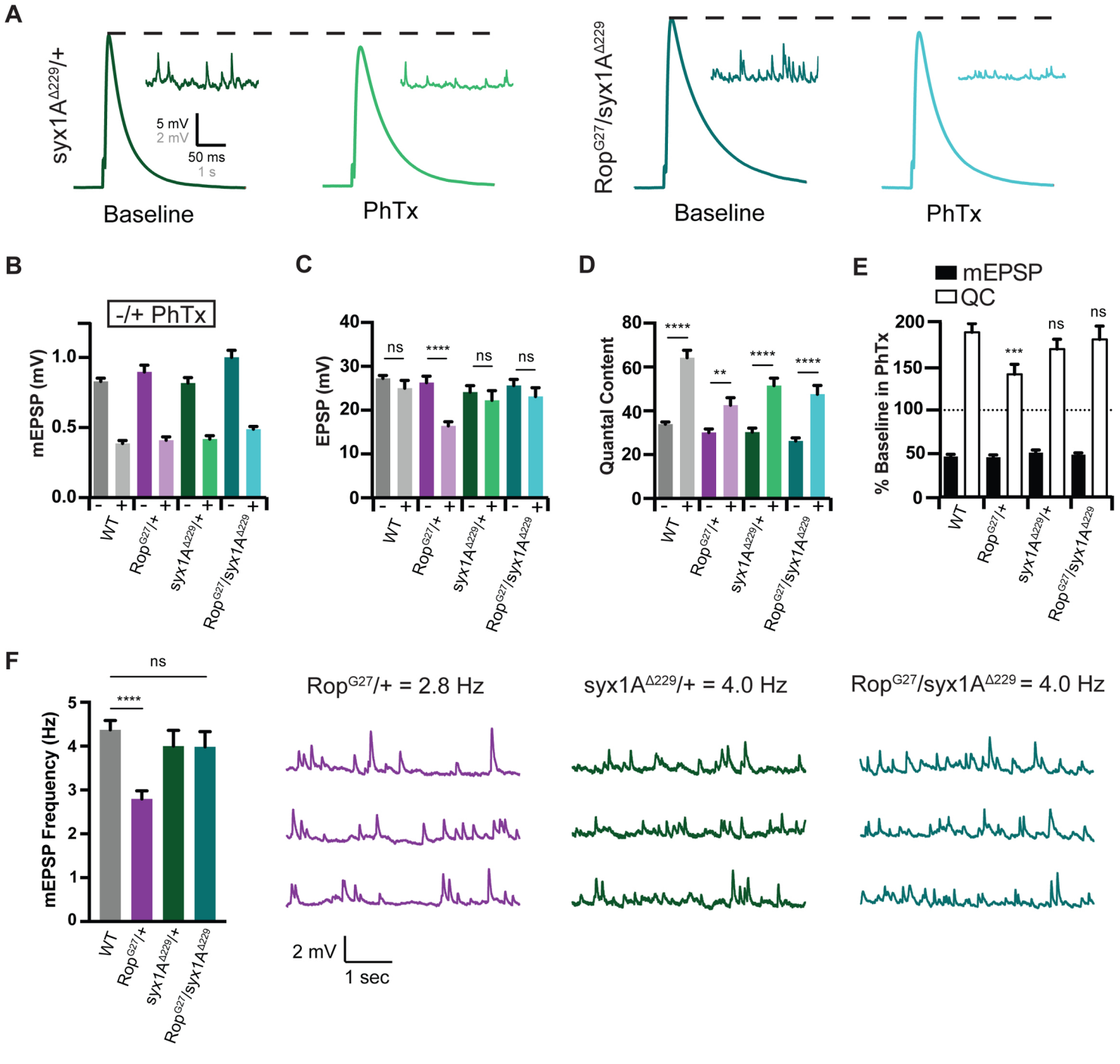
A
syx1A^Δ229/+
5 mV
2 mV
50 ms
1 s
Baseline
PhTx
Rop^G27/syx1A^Δ229
Baseline
PhTx
B
-/+ PhTx
mEPSP (mV)
1.0
0.5
0.0
- + - + - + - +
WT
Rop^G27/+
syx1A^Δ229/+
Rop^G27/syx1A^Δ229
C
EPSP (mV)
40
30
20
10
0
ns
****
ns
ns
D
Quantal Content
80
60
40
20
0
****
**
****
****
E
mEPSP
QC
% Baseline in PhTx
200
150
100
50
0
***
ns
ns
F
mEPSP Frequency (Hz)
5
4
3
2
1
0
ns
****
Rop^G27/+ = 2.8 Hz
syx1A^Δ229/+ = 4.0 Hz
Rop^G27/syx1A^Δ229 = 4.0 Hz
2 mV
1 sec

Figure 9

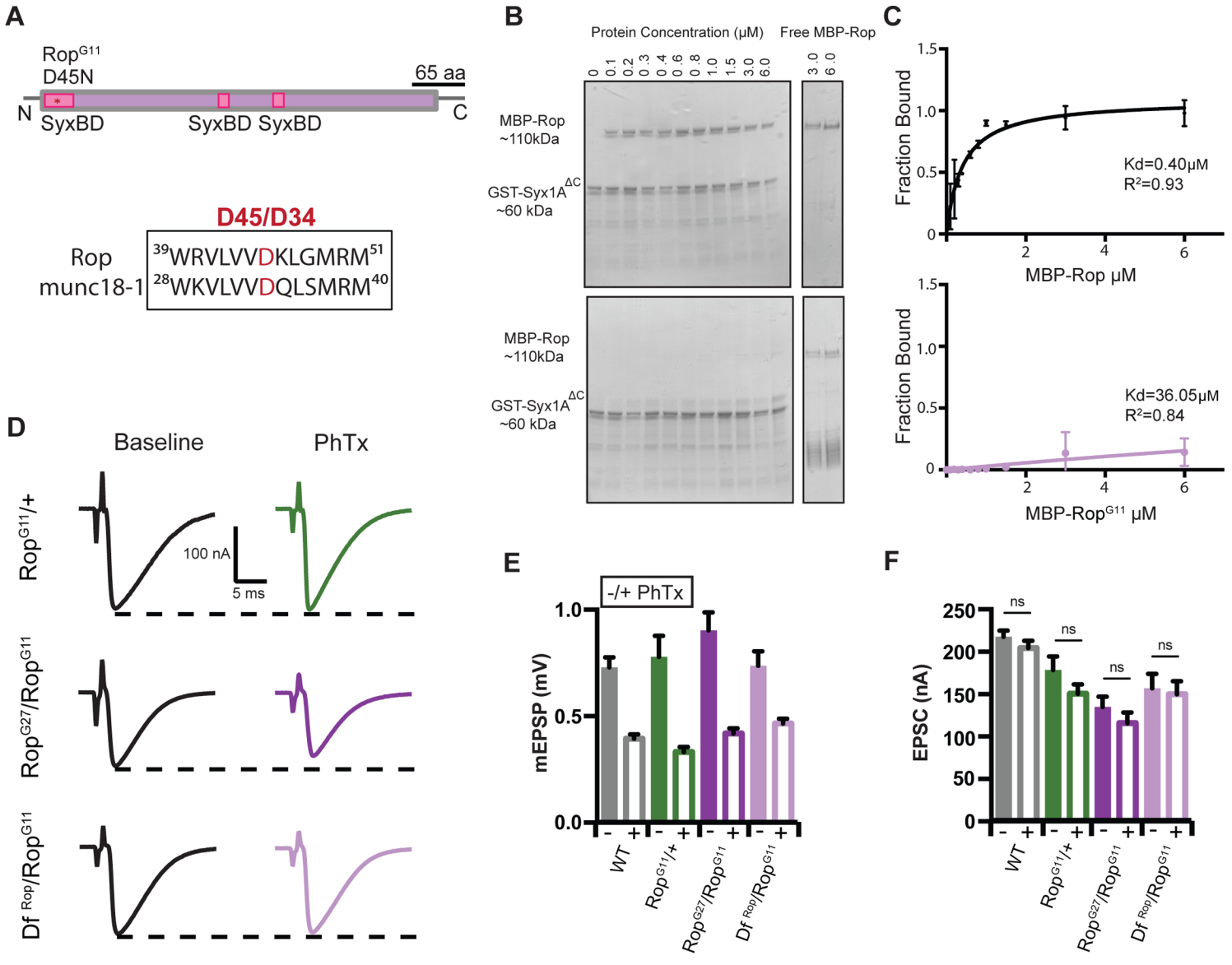
A
Rop^G11 D45N
65 aa
N
C
SyxBD
SyxBD SyxBD
D45/D34
Rop
munc18-1
39WRVLVVDKLGMRM51
28WKVLVVDQLSMRM40
B
Protein Concentration (μM)
Free MBP-Rop
0 0.1 0.2 0.3 0.4 0.6 0.8 1.0 1.5 3.0 6.0
3.0 6.0
MBP-Rop ~110kDa
GST-Syx1A^ΔC ~60 kDa
MBP-Rop ~110kDa
GST-Syx1A^ΔC ~60 kDa
C
Fraction Bound
Kd=0.40μM
R²=0.93
MBP-Rop μM
Fraction Bound
Kd=36.05μM
R²=0.84
MBP-Rop^G11 μM
D
Baseline
PhTx
Rop^G11/+
100 nA
5 ms
Rop^G27/Rop^G11
Df Rop/Rop^G11
E
-/+ PhTx
mEPSP (mV)
WT
Rop^G11/+
Rop^G27/Rop^G11
Df Rop/Rop^G11
F
EPSC (nA)
ns
WT
Rop^G11/+
Rop^G27/Rop^G11
Df Rop/Rop^G11

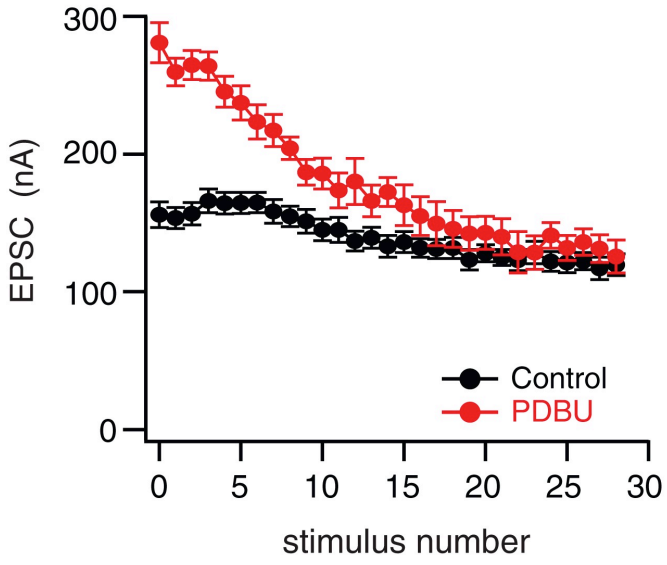

Figure 1_Supplemental Figure 1. PdBu-dependent potentiation converges to wild type steady state during a prolonged stimulus train. Average peak amplitudes of 60 Hz trains in the absence (black) and presence (red) of PdBu (n=6 for control, n=4 for PdBu, data are mean ± SEM). The average of the last three data points at the end of the stimulus trains are statistically similar ($p>0.1$; Student's t-test, two tails).